AD-A140 869 ACOUSTIC ATTENUATION IN OCEAN SEDIMENTS FOUND IN SHALLOW WATER REGIONS(U) TEXAS UNIV AT AUSTIN APPLIED RESEARCH LABS K C FOCKE 29 FEB 84 ARL-TR-84-6 1/1

UNCLASSIFIED N00014-82-K-0015 F/G 20/1 NL

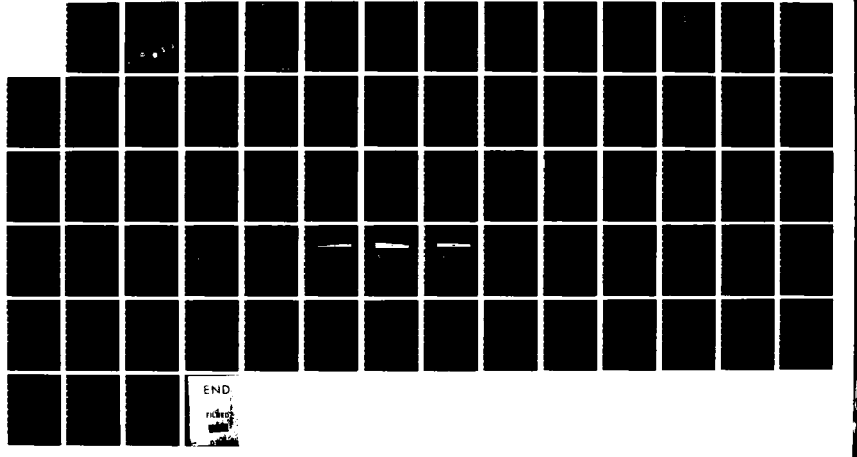

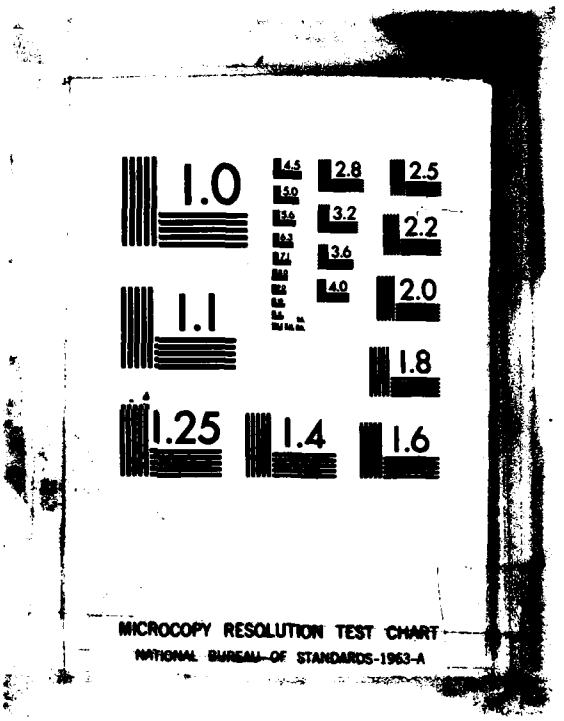
1.0
1.1
1.25
1.4
1.6
1.8
2.0
2.2
2.5
2.8
3.2
3.6
4.0
4.5
5.0
5.6
6.3
7.1
MICROCOPY RESOLUTION TEST CHART
NATIONAL BUREAU OF STANDARDS-1963-A

(12)

ARL-TR-84-6

Copy No. 41

ACOUSTIC ATTENUATION IN OCEAN SEDIMENTS FOUND IN SHALLOW WATER REGIONS

Karl Crawford Focke

APPLIED RESEARCH LABORATORIES
THE UNIVERSITY OF TEXAS AT AUSTIN
POST OFFICE BOX 8029, AUSTIN, TEXAS 78713-8029

29 February 1984

Technical Report

Prepared for:

NAVAL OCEAN RESEARCH
AND DEVELOPMENT ACTIVITY
NSTL STATION, MS 39529

UNCLASSIFIED

SECURITY CLASSIFICATION OF THIS PAGE (When Data Entered)

REPORT DOCUMENTATION PAGE		READ INSTRUCTIONS BEFORE COMPLETING FORM
1. REPORT NUMBER	2. GOVT ACCESSION NO. AD-A140 869	3. RECIPIENT'S CATALOG NUMBER
4. TITLE (and Subtitle) ACOUSTIC ATTENUATION IN OCEAN SEDIMENTS FOUND IN SHALLOW WATER REGIONS		5. TYPE OF REPORT & PERIOD COVERED Technical Report
		6. PERFORMING ORG. REPORT NUMBER ARL-TR-84-6
7. AUTHOR(s) Karl Crawford Focke		8. CONTRACT OR GRANT NUMBER(s) N00014-82-K-0015
9. PERFORMING ORGANIZATION NAME AND ADDRESS Applied Research Laboratories The University of Texas at Austin P.O. Box 8029, Austin, Texas 78713-8029		10. PROGRAM ELEMENT, PROJECT, TASK AREA & WORK UNIT NUMBERS
11. CONTROLLING OFFICE NAME AND ADDRESS Naval Ocean Research and Development Activity NSTL Station, MS 39529		12. REPORT DATE 29 February 1984
		13. NUMBER OF PAGES 68
14. MONITORING AGENCY NAME & ADDRESS(if different from Controlling Office)		15. SECURITY CLASS. (of this report) UNCLASSIFIED
		15a. DECLASSIFICATION/DOWNGRADING SCHEDULE

16. DISTRIBUTION STATEMENT (of this Report)

Approved for public release; distribution unlimited.

17. DISTRIBUTION STATEMENT (of the abstract entered in Block 20, if different from Report)

18. SUPPLEMENTARY NOTES

19. KEY WORDS (Continue on reverse side if necessary and identify by block number)

Shallow water
Acoustic propagation
Acoustic attenuation

20. ABSTRACT (Continue on reverse side if necessary and identify by block number)

The acoustic attenuation in ocean sediments is a major loss mechanism for low frequency acoustic propagation in shallow water regions. Analysis of measured propagation in these regions has generally included estimates of the attenuation in the sediment, without consideration of the variations in attenuation as a function of depth. It will be shown that these variations can have a significant impact on the standard estimates. A new procedure is then developed which provides estimates of the attenuation as a function of depth. This procedure is used to obtain attenuation depth profiles in three

DD FORM 1 JAN 73 1473 EDITION OF 1 NOV 65 IS OBSOLETE

20. (Cont'd)

shallow water regions. These estimated profiles present characteristics observed in laboratory and in situ measurements.

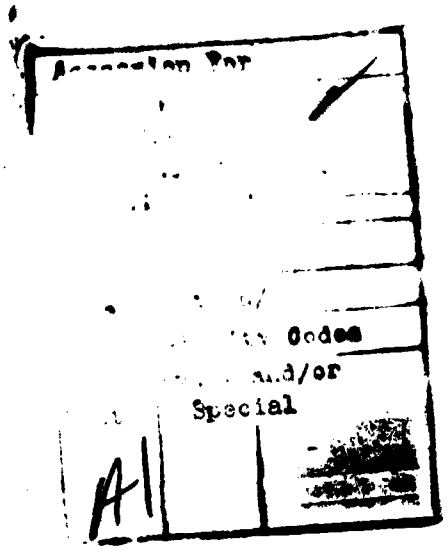

TABLE OF CONTENTS

		Page
LIST OF FIGURES		v
I.	INTRODUCTION	1
	A. Shallow Water	1
	B. Background	3
	C. Summary of the Report	5
II.	OCEAN SEDIMENT ATTENUATIONS	10
	A. Properties of Sediment Attenuation	10
	B. Acoustic Modeling for Shallow Water	13
	C. Effects of Depth Variations	18
III.	ESTIMATING THE ATTENUATION PROFILE	26
	A. Input Parameters	26
	B. Frequency Characteristics of the Normal Modes	27
	C. Estimating the Attenuation Profile	32
IV.	ATTENUATION PROFILES IN EXAMPLE SHALLOW WATER REGIONS	39
	A. Environmental Descriptions	39
	B. Measured Propagation Loss	43
	C. Attenuation Profiles	44
	D. Conclusions and Recommendations	50
REFERENCES		52
RELATED PUBLICATIONS		57

LIST OF FIGURES

Figure		Page
I.1	Comparison of Measured and Predicted Arrival Structure in Deep Water	4
I.2	Envelope of Shot in 1/3 Octave Bands Propagated over a Clay Bottom	6
I.3	Envelope of Shot in 1/3 Octave Bands Propagated over a Sand Bottom	7
II.1	Compressional Wave Attenuation Profiles for Shallow Water Sediments	20
II.2	Sediment Attenuations $\alpha'(f)$ Calculated using Eq. II.11 for the Attenuation Profiles Given in Fig. II.1	21
II.3	Compressional Wave Attenuation Profile for a Sand Sediment	23
II.4	Comparison of Calculated Attenuations $\alpha'(f)$ for the Attenuation Profile in Fig. II.3 and Data from Ref. 17	24
II.5	Comparison of Calculated Depth-Constant Attenuations for the Modified Version of Profile 1, Fig. II.1, and Results from Ref. 16	25
III.1	Environmental Description and Mode 1 at 50 Hz and 400 Hz for a Shallow Water Area	30
III.2	Distribution of Mode Quantities in the Sediment for Mode 1 at 50 Hz and 400 Hz. (---) Relative Amplitude of the Mode Function, (—) Integral of the Mode Function Squared. Clay-Silt Bottom.	31

Figure		Page
III.3	Distribution of Mode Quantities in the Sediment for Mode 1 at 50, 400, and 1600 Hz. (---) Relative Amplitude, (—) Integral of Mode Function Squared. Sandy Bottom.	33
III.4	Attenuation Profile Generated by Frequency Considerations	35
III.5	Comparison Between Input and Estimated Attenuation Profiles	37
III.6	Propagation Loss Comparison Between Input and Calculations Based on Estimated Attenuation Profile	38
IV.1	Bathymetry and Measured Propagation Loss for Site 1	40
IV.2	Bathymetry and Measured Propagation Loss for Site 2	41
IV.3	Bathymetry and Measured Propagation Loss for Site 3	42
IV.4	Comparison of Calculated and Measured Propagation Loss at Site 1	45
IV.5	Comparison of Calculated and Measured Propagation Loss at Site 2	47
IV.6	Estimated Attenuation Profile for Site 3	48
IV.7	Comparison of Calculated and Measured Propagation Loss at Site 3	49

CHAPTER I
INTRODUCTION

This report grew out of work at Applied Research Laboratories, The University of Texas at Austin (ARL:UT), in ocean acoustics, specifically acoustic propagation between source and receiver located in the water. In shallow water regions this propagation involves a significant amount of interaction with the seafloor. This interaction affects the amount of loss of signal level incurred as a signal propagates from source to receiver. This report considers the acoustic attenuation in the seafloor sediments and the effects this attenuation has on acoustic propagation in shallow water. Also presented is a preliminary technique for estimating these attenuations as a function of both acoustic frequency and sediment depth. This technique does not require physical sampling of the seafloor, but uses acoustic field measurements.

The estimates of the attenuation in the sediments become part of a geoacoustic description[1] of the measurement region. These geoacoustic descriptions, comprised of sound speed, attenuation, and density, together with water mass parameters, are used to numerically compute acoustic propagation in the water. These calculations can provide propagation loss for source depths, receiver depths, and frequencies not covered in the measurements, thus providing a complete acoustical analysis of the measurement region.

A. Shallow Water

In ocean acoustics the term "shallow water" has been given different definitions by different authors. Brekhovskikh[2] and Tolstoy and Clay[3] define shallow water in terms of the wavelength of sound at the frequencies of interest. Other authors, such as Officer,[4] define

shallow water by a physical water depth. The definition of shallow water used in this report was obtained by first considering the frequencies of interest in related research at ARL:UT[5,6] and then choosing a specific depth as the maximum depth to be considered. The frequencies of interest range from a few tens of hertz up to 2000 Hz. Within this frequency range the compressional wave attenuation is the dominant loss mechanism in the sediment. For this application, the definition of shallow water has been chosen based on the wavelengths of the lower frequencies. The characteristic depth was chosen to be 500 m and shallow water is identified as those regions of water depth less than 500 m.

This shallow water definition includes not only the continental shelves, but also the shallow seas which border the continental margins. These regions are regions of variability. Major variations occur in the water depth, water mass, and bottom composition. These variations will occur within a region, as well as between regions. The variations in the environment result in variations in the acoustic propagation.[7] Seasonal changes in the sound speed profile, changes or differences in water depth, and differences in bottom composition all affect the propagation by modifying the bottom interactions. When the seasonal changes result in increased bottom interaction, the propagation losses increase.

In shallow water where the bottom has a significant impact on the propagation, variations in the sediment parameters should not be ignored in an analysis of the region. In particular, the variations in attenuation within the first 50 m of sediment can affect propagation. Previous authors have ignored depth variability in attenuation. Those authors concluded that the attenuation was not linearly related to frequency. They also concluded that shear wave excitation was an important loss mechanism; however, shear wave speeds significantly greater than those measured in the sediments were required in their analyses. Ignoring the depth variability of attenuation can therefore result in incorrect interpretation of the frequency dependence of the attenuation.

B. Background

The idea of developing a procedure for estimating the attenuation profile in shallow water regions grew out of the analysis of acoustic propagation in deep water.[5,8] Methods for measuring the attenuation profile in deep ocean sediments were developed to aid analysis of acoustic propagation data. The resulting attenuation profiles were then used in the acoustic description of the sediments in the measurement regions. As the remainder of this report will show, it is necessary to use an attenuation profile in the acoustic description of the sediment. Therefore a method was needed to estimate the attenuation profiles in these shallow water regions using the measured propagation data.

Hamilton[9] has compiled results from acoustic measurements which show that attenuation does vary with depth into the sediment. A significant contribution to this compilation was based on work presented by Neprochnov,[10] who was able to analyze deep ocean propagation data in terms of the depth variations in the acoustic properties. Following Hamilton, Mitchell and Focke[5] and later Jacobson et al.[11] have presented measured attenuation profiles in deep ocean sediments.

Neprochnov, unfortunately, did not present the method used to obtain his results. However, both Mitchell and Focke and Jacobson et al. did discuss the methods involved. Although these two procedures differed, both techniques were based on multipath analysis. The received signal from an impulsive source can be time separated into multipath arrivals, each with identifiable ray path histories. Figure I.1 is an example of a received signal recorded in deep water.[8] Also presented in this figure are the predicted ray arrivals and the associated ray path histories. The histories include the number of bottom bounces, the bottom grazing angle, and a reference loss. Measured values presented in the figure include the measured loss and the loss per bottom bounce (bottom loss) for each arrival.

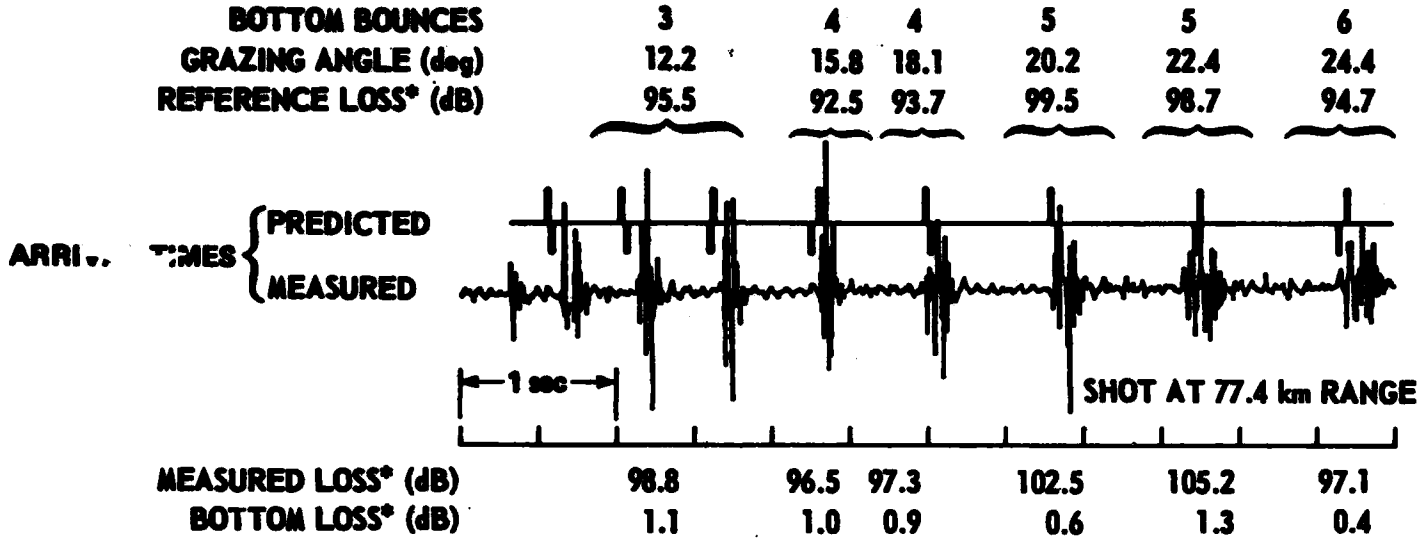

*AT 50 Hz

FIGURE I.1
COMPARISON OF MEASURED AND PREDICTED ARRIVAL STRUCTURE IN DEEP WATER

The bottom loss values contain information about the attenuation profile in the sediment. Given a sound speed profile in the sediment, ray paths through the sediment can be identified. The bottom losses then provide estimates of the energy lost along each path, and path lengths obtained from ray tracing yield estimates of the attenuation profile.

These deep water methods can be seen to depend upon the time separability of the received signals. To apply these procedures to shallow water data would require a time separability in the data. Figure I.2 presents a signal received in a shallow water region with a clay sediment. At 50 Hz the signal is composed of overlapping arrivals and the total received signal spans a time of approximately 4.5 sec. At 200 Hz, the signal presents a different structure; there is one significant peak and the total duration is approximately 2.0 sec.

Figure I.3 presents a received signal in shallow water which has propagated over a sand bottom. The source waveform is composed of an initial pressure impulse followed by three secondary impulses at intervals of approximately 40 msec. At both 100 and 400 Hz, the received signal is made up of a single arrival with this pulsed waveform.

In both shallow water cases above, the multipath structure required by the deep ocean attenuation analysis procedures is not present. General ray theory representation of propagation used in those procedures cannot describe the characteristics seen in the data. To estimate the attenuation from propagation data, the propagation needs to be analyzed by a wave theory model, such as a normal mode model. The problem in estimating the profile will be associating measured propagation characteristics with depth dependent mode characteristics.

C. Summary of the Report

The remainder of this report is divided into three chapters. Chapter II is on acoustic attenuation in the sediments. Chapter III

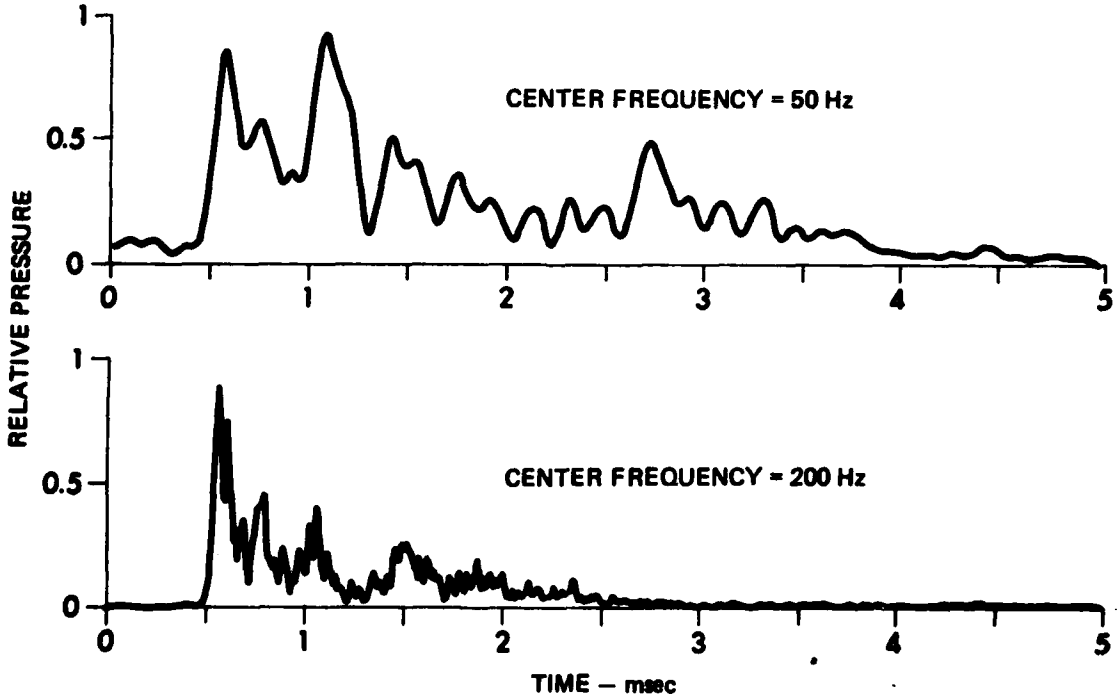

FIGURE I.2
ENVELOPE OF SHOT IN 1/3 OCTAVE BANDS
PROPAGATED OVER A CLAY BOTTOM
RANGE = 36 km, SOURCE DEPTH = 91 m,
RECEIVER DEPTH = 305 m

ARL:UT
AS-82-1592
KCF-GA
10-6-82

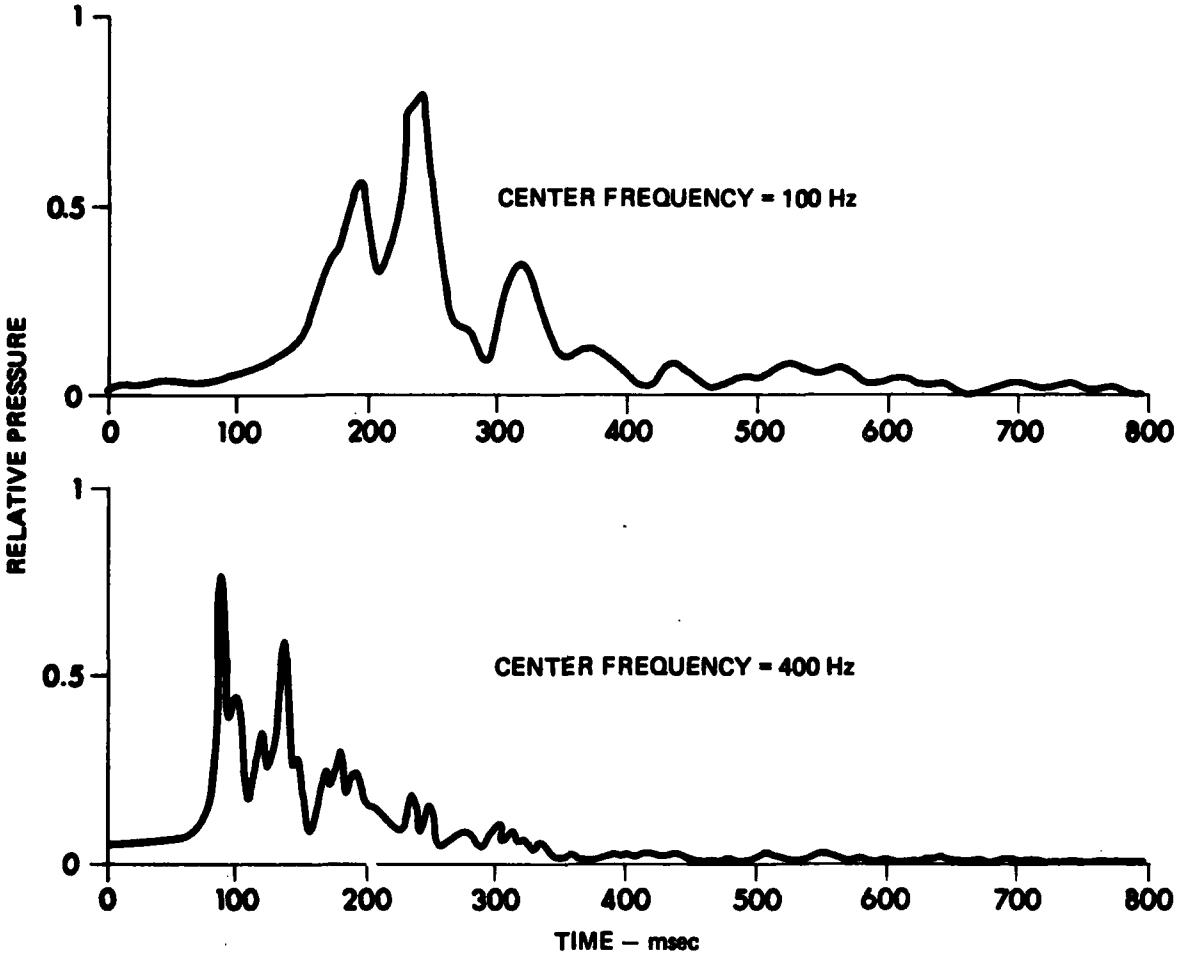

FIGURE I.3
ENVELOPE OF SHOT IN 1/3 OCTAVE BANDS
PROPAGATED OVER A SAND BOTTOM
RANGE = 158 km, SOURCE DEPTH = 91 m,
RECEIVER DEPTH = 110 m

presents the preliminary technique for estimating the attenuation profile. Finally, attenuation profiles are estimated for three measurement regions in Chapter IV.

The discussion on attenuation in Chapter II notes that there are two points of view on the variability of the attenuation. The point of view taken in this report is based on measured results: the attenuation varies linearly with frequency and it varies with depth. The method for including the sediment attenuation in the calculation of propagation loss is also presented. Calculations are then used to demonstrate how a nonlinear frequency dependence of attenuation can be obtained if depth variations in the attenuation are ignored.

The technique for estimating the attenuation profile as presented in Chapter III is based on the normal mode theory and uses propagation loss measured at several frequencies. Shallow water propagation in the frequency range below approximately 2 kHz, beyond a few water depths, involves only the low order normal modes. For these modes, there is a correlation between the acoustic frequency of the propagating signal and the amount of penetration into the sediment. At the high frequencies, the modes penetrate only the surface layer. As the frequency decreases, the modes penetrate to the deeper layers. By calculating the normal modes and determining a depth of penetration as a function of frequency, attenuation values are estimated as a function of depth.

In Chapter IV attenuation profiles are estimated for three shallow water regions. In each region the attenuation values were within the range specified by Hamilton for the sediment types found in the measurement regions. In the sand sediment, the attenuation was found to decrease with depth. Again, this result was in agreement with laboratory results[12] and theoretical results.[13] In the clay regions, one profile was found to increase with depth while the other profile decreased with depth. Based on a compilation of measured results,[9] the attenuation in homogeneous clay sediments generally is expected to increase with depth.

The differences between the two estimated profiles and the generally expected results were, however, in agreement with large variability of attenuation in these sediment types.

These linear frequency dependent compressional attenuation profiles were sufficient to account for the frequency characteristics seen in the measured propagation loss results. Additional loss mechanisms, such as shear waves in the sediments, were not required. Accurate modeling of the acoustic propagation and an understanding of the acoustic interactions with the bottom resulted in attenuation profiles which agreed with previously reported results.[9]

CHAPTER II
OCEAN SEDIMENT ATTENUATIONS

The compressional wave attenuation due to the seafloor sediments can have a significant influence on acoustic propagation in shallow water. At low frequencies, where the sediment is the only significant source of attenuation, this parameter determines how rapidly propagating acoustic signals decay with range. Before discussing a method of estimating these attenuations, the attenuation in the sediment should be discussed. This will provide an understanding of the characteristics of the attenuation including the range of values to be expected. There will also be a discussion on how attenuation enters into the propagation loss calculations since these calculations are often used to obtain estimates of attenuation. There will also be a discussion on the effects of ignoring certain characteristics of the attenuation in terms of data analysis results.

A. Properties of Sediment Attenuation

Acoustic compressional wave attenuation within a sediment varies with acoustic frequency, with depth into sediment, and with sediment type.[9] How the characteristics of attenuation are related to each of these parameters is of interest in estimating the attenuation profile since the interplay between these relationships contribute to the frequency dependence of the propagation. The effects on propagation resulting from attenuation varying with depth and frequency are interrelated, and an estimate of one relationship is dependent upon assumptions about the other. A knowledge of the variations with sediment type are of interest when estimates are obtained; that is, if the estimates are to be accepted, they need to be consistent with values expected for the sediment type. How the attenuation actually varies with

each of these parameters has not been fully established. There are basically two points of view: one based on in situ measurements, and the other based on theoretical considerations. They differ in some very important ways.

The relationship between the acoustic frequency and the sediment attenuation is one point of controversy. The mathematical models based on the theoretical work of Biot,[14] Stoll and Bryan,[15] and Stoll,[13] consider two loss mechanisms: frictional losses between the grains and fluid viscous losses of the pore fluid. The model predicts a linear relation between frequency and frictional attenuation. For the viscous losses, however, the model predicts a relationship that changes from f^2 at low frequency to $f^{1/2}$ at high frequency. In the frequency range of interest, the actual relationship between the total attenuation and frequency will be a combination of these two mechanisms and is dependent upon the sediment type.

For sediments of high porosity (relative volume of the fluid, given in percentages), such as clays and silts, the frequency-attenuation relationship is almost linear. For low porosity sediments, such as sands, the viscous losses dominate the attenuation and the model predicts an f^2 relationship in the low end of our frequency range, changing to an $f^{1/2}$ relationship at high frequencies. The specific relationship at any selected frequency is dependent upon the grain size.

Interpretation of experimental acoustic propagation measurements have indicated nonlinear relationships between frequency and attenuation given as

$$\alpha = Kf^n \quad . \qquad \text{II.1}$$

Based on propagation loss measurements, Rubano[16] found the attenuation to be proportional to the 1.1 power of frequency (n=1.1). Ingenito,[17]

also working with propagation loss data, found attenuation related to the 1.75 power of frequency (n=1.75). Analyses of acoustic propagation data, using the Biot-Stoll model to provide the sediment attenuation, have resulted in similar relationships.[18] The analyses leading up to the nonlinear relationships have not considered depth variations in the attenuation. As will be shown later, this oversight can lead to erroneous interpretations.

The theoretical work of Biot[14] assumed a uniform spherical pore size. Hovem[19] has shown that the attenuation-frequency relationship, due to viscous losses, is dependent upon this assumption. Using a modified suspension model, where calculations are made as the grains were in suspension and there is no effect of intergrain contact, Hovem showed that for mixed grain sizes the attenuation tends toward a linear relationship with frequency over a broad frequency range, while still agreeing with the Biot model for uniform grain sizes.

Hamilton has compiled and analyzed as many as possible of the attenuation measurements taken in unlithified marine sediments.[9] He found that the attenuation is approximately linear with frequency. Unfortunately there is a paucity of data in the frequency range 10-1000 Hz, and one may need to rely upon the modeling to fill the gaps. Fortunately, the result of Hovem indicating that a linear relationship can be assumed across our entire frequency range is in agreement with the data.

At any given frequency, the attenuation in different sediments is found to vary by at least an order of magnitude. Assuming a linear frequency dependence, Hamilton was able to exhibit an attenuation dependence related to sediment type. The general trend is for the attenuation to increase with decreasing porosity. It ranges from 0.01-0.10 dB/kHz-m for clays up to 0.2-0.9 dB/kHz-m for sands.

In addition to variations with the acoustic frequency and the sediment type, sediment attenuation also varies with depth into the sediment. Stoll[13] investigated the effects of depth on the attenuation by varying the overburden pressure in his theoretical model. He found the attenuation decreases with increasing pressure or depth. The variations he did find, however, were relatively small in the frequency range between 10 and 1000 Hz, decreasing by approximately 15% over a 100 m depth change. Laboratory measurements in sand sediments[12] confirm this decrease, although the attenuation measurements show 55% of change for the same depth change. For the high porosity sediments, however, the attenuation measurements reported by Hamilton show a general increase with depth in the first 400-600 m of sediment. In these sediments, the increase in overburden pressure is accompanied by a decrease in the porosity as the depth increases. The change in the porosity leads to the increase in attenuation.

There are two viewpoints on sediment attenuation, that differ on how attenuation varies with frequency and depth. Acoustic analysis which have supported the Biot-Stoll model have ignored the possible influence of the depth variations, and it will be shown later how this can lead to erroneous conclusions about the frequency dependence. The point of view taken in this report is guided by the measurements. The attenuation is assumed to vary linearly with the acoustic frequency and to vary with depth into the sediment.

B. Acoustic Modeling for Shallow Water

The estimation procedure developed in the next chapter is based on the interpretation of measured propagation loss using a propagation model. To understand the procedure, one needs to know how the model accounts for the sediment attenuation. For the purpose of estimating environmental parameters from acoustic propagation data, there are basically two ways to describe the acoustic propagation: ray theory and normal mode theory. Both theories have been applied to

numerical modeling of the propagation in shallow water,[20,21] although at frequencies below 1000 Hz the normal mode theory is more widely used.

Shallow water presents difficulties to the ray theory approach. In the vicinity of the water-sediment interface, the basic ray theory assumptions are invalid.[3] In shallow water the entire water column is in the vicinity of this interface for the low frequencies. The standard procedure around this limitation is to replace the sediment with a plane wave reflection coefficient. However, at low frequencies in shallow water, the plane wave reflection is not always adequate, and additional corrections are needed to account for the non-plane wave nature of the propagation.[22,23]

Acoustic propagation in shallow water can be expressed by the solution to the separated homogeneous wave equation when horizontal stratification and azimuthal symmetry are assumed. For a harmonic time dependent source, the acoustic field at a depth z and range r from the source at depth z_o is expressed as

$$\phi(r,z) = \sum_n \psi_n(z_o)\, \psi_n(z)\, H_o^{(1)}(k_n r) \quad , \qquad \text{II.2}$$

where $H_o^{(1)}(k_n r)$ is the Hankel function of the first kind, $\psi_n(z)$ is the nth mode or eigenfunction of the vertical component of the particle velocity, and k_n is the eigenvalue. The propagation loss can be expressed as

$$PL(r,z) = -10 \log_{10}\left\{\frac{1}{r}\frac{2}{\pi}\left|\sum_n k_n^{-1/2}\, \psi_n(z_o)\, \psi_n(z)\, e^{ik_n r}\right|^2\right\} \quad , \qquad \text{II.3}$$

where the asymptotic form of $H_o^{(1)}(k_n r)$ has been used. The 1/r term results from $H_o^{(1)}(k_n r)$ and represents cylindrical spreading of the modes. Range also appears in the exponents, $ik_n r$. Writing the eigenvalue k_n as

$$k_n = \kappa_n + i\delta_n \quad , \qquad \text{II.4}$$

the exponents in Eq. II.3 become $(-\delta_n r + i\kappa_n r)$, where $\delta_n r$ is the mode attenuation and $\kappa_n r$ is the mode phase. An increase in range increases $\delta_n r$ for each n, which leads to a general increase in PL(r,z). However, small changes in range can also result in large phase differences between the modes. This can result in constructive or destructive interference of the modes, and within small range intervals PL(r,z) can vary as much as 15 dB. These fluctuations in PL(r,z) can easily obscure the general trends resulting from cylindrical spreading and mode attenuation.

Propagation loss measurements are often made using explosive shots and are evaluated within selected frequency bands. The frequency averaging, represented by these frequency band measurements, eliminates most of the fluctuations in the propagation loss resulting from the mode interference. These measurements can usually therefore be characterized by cylindrical spreading and attenuation.

The mode interference can easily be removed from the calculations (Eq. II.3) by expressing the propagation loss as an incoherent sum of the modes

$$PL(r,z) = -10 \log_{10} \left\{ \frac{2}{\pi r} \sum \left(\left| k_n^{-1/2} \phi_n(z_o) \psi_n(z) e^{-\delta_n r} \right|^2 \right) \right\} \quad . \qquad \text{II.5}$$

Equation II.5 defines propagation loss as a monotonically increasing function of range which can be characterized by cylindrical spreading and mode attenuation.

The calculation of acoustic propagation now involves the determination of k_n and ψ_n. If shear waves are not considered, the depth component of the wave equation takes the form

$$\frac{d^2\psi_n(z)}{dz^2} + \left[k^2(z)-k_n^2\right]\psi_n(z) = 0 \quad , \qquad \text{II.6}$$

where k(z) is the propagation wave number. The solutions to Eq. II.6 must also satisfy the boundary conditions

$$\psi_n(0) = 0 \quad ,$$

$$\left.\frac{\partial\psi_n(z)}{\partial z}\right|_{z=H_i^-} = \left.\frac{\partial\psi_n(z)}{\partial z}\right|_{z=H_i^+} \quad , \qquad \text{II.7}$$

$$\left.\rho(z)\psi_n(z)\right|_{z=H_i^-} = \left.\rho(z)\psi_n(z)\right|_{z=H_i^+} \quad ,$$

where the H_i's designate the horizontal boundaries. These conditions result from a pressure release surface condition, and continuity of pressure and normal component of particle velocity at each horizontal boundary identified by a change in density. The Sommerfeld radiation condition is also imposed on the solution to allow only outward propagation at infinite depth.

Equation II.6 will take into account attenuation in the medium when k(z) is defined as a complex function

$$k(z) = \frac{\omega}{c(z)} + i\alpha(z) \quad , \qquad \text{II.8}$$

where $\alpha(z)$ is the attenuation, c(z) is the sound speed, and ω is the acoustic angular frequency. In this case both $\psi_n(z)$ and k_n will also be complex. The mode attenuation coefficient δ_n is defined as the imaginary part of k_n, as in Eq. II.4.

Following Schiff[24] and Koch et al.,[25] a perturbation solution for δ_n can be developed in terms of $\psi_n(z)$ and κ_n. This approach is based on the assumption that $\alpha(z) << \omega/c(z)$. The attenuation is introduced as a slight perturbation to the environment with the effect of producing a slight perturbation to k_n and ψ_n. Equation II.6 is rewritten by substituting Eq. II.8 for k(z), Eq. II.4 for k_n, $(\kappa_n + \Delta\kappa_n)$ for κ_n, and $(\psi_n + \Delta\psi_n)$ for ψ_n. This new Eq. II.6 is expanded and all terms with two or more perturbation parameters are dropped. This final differential equation is linear with respect to the perturbation parameters. By integrating this equation, δ_n can be expressed as

$$\delta_n = \frac{\omega}{\kappa_n I_n} \int \rho(z) \frac{\alpha(z)}{c(z)} \left|\psi_n(z)\right|^2 dz \quad ,$$

$$I_n = \int \rho(z) \left|\psi_n(z)\right|^2 dz \quad , \qquad \text{II.9}$$

where I_n is the normalization factor for the nth mode. The perturbed solutions for κ_n and $\psi_n(z)$ are the same as those calculated without considering attenuation.[24,25] The mode attenuation coefficients δ_n are therefore expressed in terms of the zero attenuation solutions.

Sediment attenuations can be handled by solving Eq. II.6 without attenuation, calculating δ_n by Eq. II.9, and defining a new eigenvalue by Eq. II.4.

C. Effects of Depth Variations

The effects of the fact that the attenuation varies with depth can be examined by looking at Eq. II.9. When the sediment attenuation is assumed to be constant with depth, Eq. II.9 simplifies to

$$\delta_n = \alpha_{sed}\gamma_{n1} + \alpha_{sub}\gamma_{n2} \quad ,$$

$$\gamma_{n1} = \frac{\rho_{sed}\omega}{\kappa_n I_n} \int_{sed} \left|\psi_n(z)\right|^2 c(z)^{-1}\, dz \quad , \qquad \text{II.10}$$

$$\gamma_{n2} = \frac{\rho_{sub}\omega}{\kappa_n I_n} \int_{sub} \left|\psi_n(z)\right|^2 c(z)^{-1}\, dz \quad ,$$

where the subscripts "sed" and "sub" denote properties of the bottom sediment and the substrate underlying the sediment, respectively. Except for thin sediments, the contribution from the substrate γ_{n2} can be ignored for the low order modes. Experimental measurements of mode attenuation coefficients $\hat{\delta}_n$ can be used to estimate the attenuation in the sediments[16-18,26,27] by

$$\alpha'(f) = \hat{\delta}_n/\gamma_{n1} \quad . \qquad \text{II.11}$$

Equation II.11 can result in attenuation estimates which are not linear with frequency. This can be illustrated for a hypothetical environment by calculating the mode attenuation coefficient according to Eq. II.9 and then estimating the sediment attenuation by Eq. II.10. Two

attenuation profiles, typical of clays, were used as examples (Fig. II.1). Both have a value of 0.03 dB/m-kHz in the first 2 m, and yet they yield significantly different power laws for δ_n in the 50-800 Hz region. The coefficients δ_1 were computed using Eq. II.9 at frequencies of 50, 100, 200, 400, and 800 Hz with a linear relation of attenuation to frequency. The required ψ_1's and κ_1's were calculated using the computer program NEMESIS.[28,29] The δ_1's were treated as if they were measured data and converted to equivalent constant-depth attenuation $\alpha'(f)$ by Eq. II.11. The results are presented by the points in Fig. II.2. Also, the actual attenuation at the sediment surface is shown by the solid line. The least square error curves (indicated by the dashed lines in Fig. II.2) for these points were

$$\alpha_1 = 29.5\ f^{1.13}\ \text{dB/km} \quad , \qquad \text{II.12}$$

with a mean square error of 0.09 $(\text{dB/km})^2$ for profile 1, and

$$\alpha_2 = 33.0\ f^{0.74}\ \text{dB/km} \quad , \qquad \text{II.13}$$

with a mean square error of 0.03 $(\text{dB/km})^2$ for profile 2. The frequencies are in kilohertz in Eqs. II.12 and II.13.

The frequency dependence of α', determined by Eq. II.11, can be strongly affected by the depth dependence of the actual attenuation. For an attenuation profile which increases with depth, α' at the lower frequencies is greater than the attenuation at the sediment surface. This would lead to n in Eq. II.1 being less than 1. When the attenuation profile decreases with depth, α' at the lower frequencies is less than the attenuation at the sediment surface. This would lead to n being greater than 1.

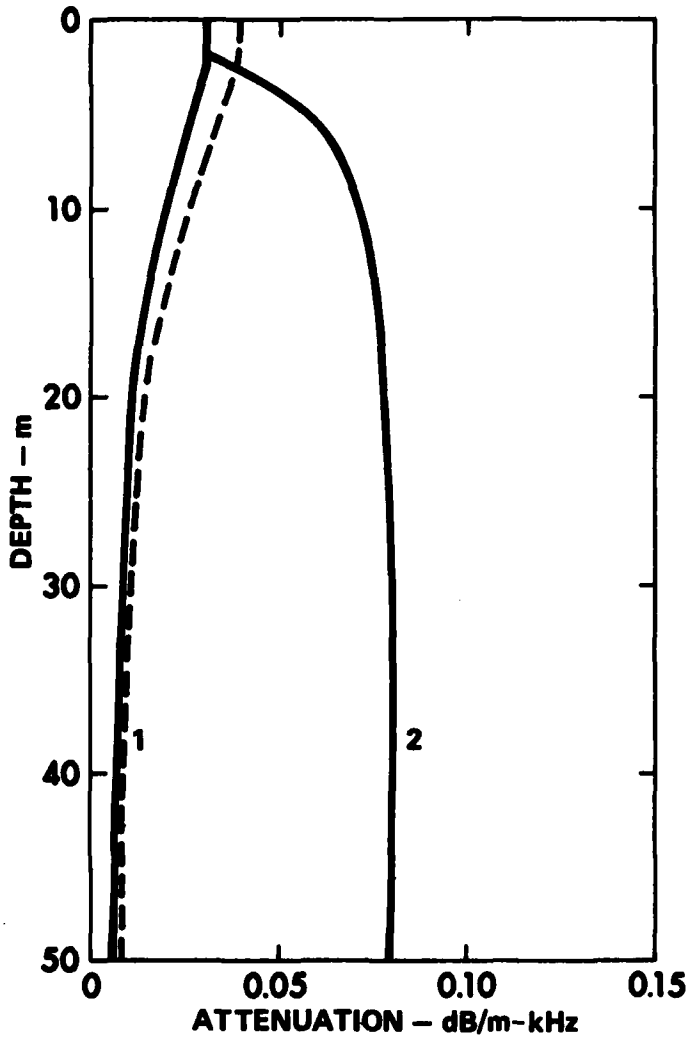

FIGURE II.1
COMPRESSIONAL WAVE ATTENUATION PROFILES FOR SHALLOW WATER SEDIMENTS

ARL:UT
AS-81-1105
KCF - GA
8 - 21 - 81

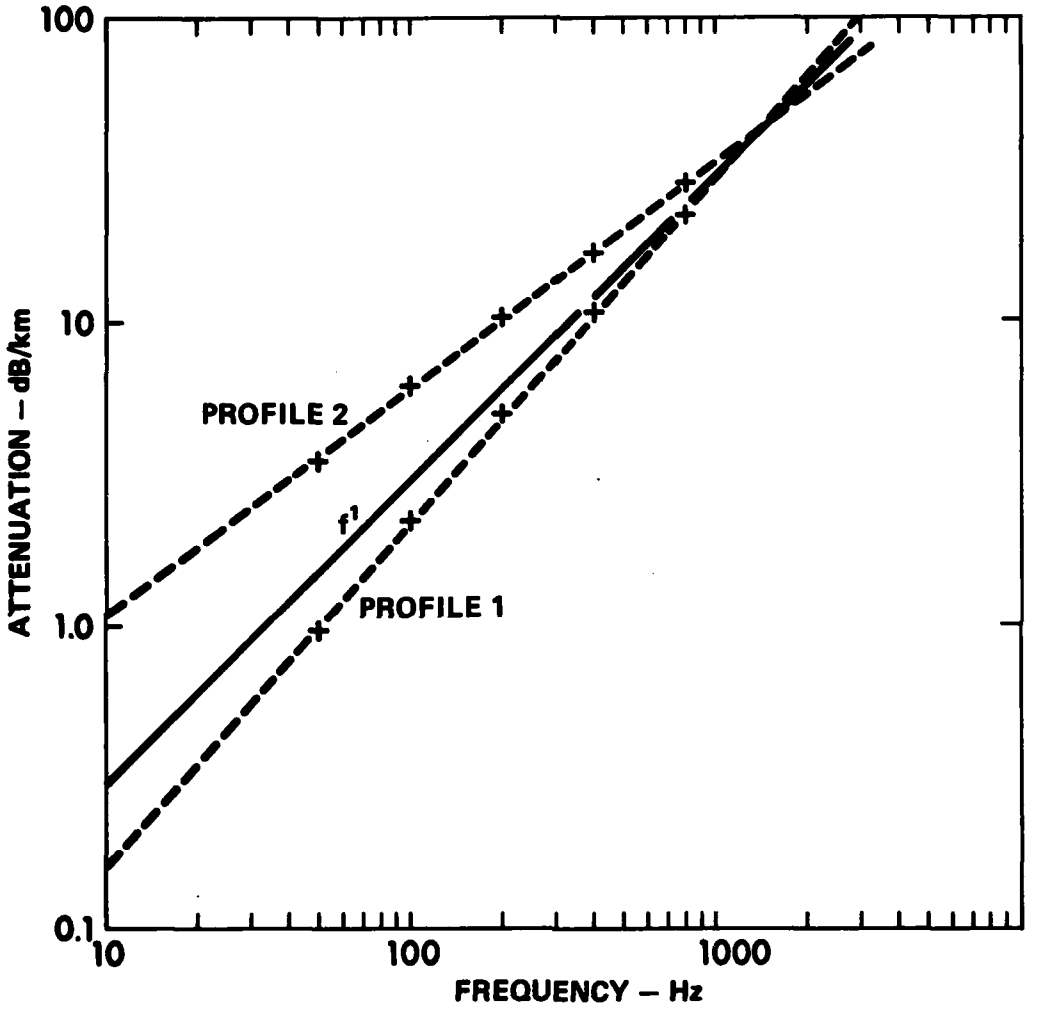

FIGURE II.2
SEDIMENT ATTENUATIONS $\alpha'(f)$ CALCULATED USING Eq. II.11 FOR THE ATTENUATION PROFILES GIVEN IN Fig. II.1

ARL:UT
AS-81-1106
KCF - GA
8 - 21 - 81

Ingenito[17] found n=1.75 while Rubano[16] found n=1.1, which would suggest attenuation profiles which decrease with depth. Ingenito worked in a region with a sandy bottom. It has already been mentioned that attenuation is expected to decrease with depth for a sandy bottom.

The environmental description discussed in Ref. 17 and references therein were used along with the attenuation in Fig. II.3 to compute the mode attenuation coefficients at 400 and 750 Hz. A linear relationship between attenuation and frequency was also assumed. Equation II.11 was used to compute α' for each frequency, which was then compared to the values reported by Ingenito (Fig. II.4). The calculated values result in n=1.22. Slight changes could be made in the attenuation near the surface to increase the mode attenuation at 750 Hz while leaving 400 Hz virtually unchanged, thus increasing the apparent power law. However, the calculated values do fall within the error bars reported with the measurements showing that an attenuation profile, linearly dependent on frequency, can explain the measurements.

The frequency dependence reported by Rubano closely matches the results in Fig. II.2 for profile 1. Using the dashed curve in Fig. II.1 to define an attenuation profile and the environmental description in Ref. 16, α's were computed at 50, 100, and 400 Hz. Figure II.5 presents a comparison between these calculations and the results reported by Rubano. The largest difference was 0.35 dB/km at 400 Hz. Here again, an attenuation profile, linearly dependent on frequency, can explain the measured results.

Propagation loss measurements, such as those of Rubano and Ingenito, can provide estimates of attenuation profiles in the sediment which are linearly dependent on frequency. In the next chapter a technique for estimating these profiles is developed based on propagation loss measurements collected at numerous frequencies.

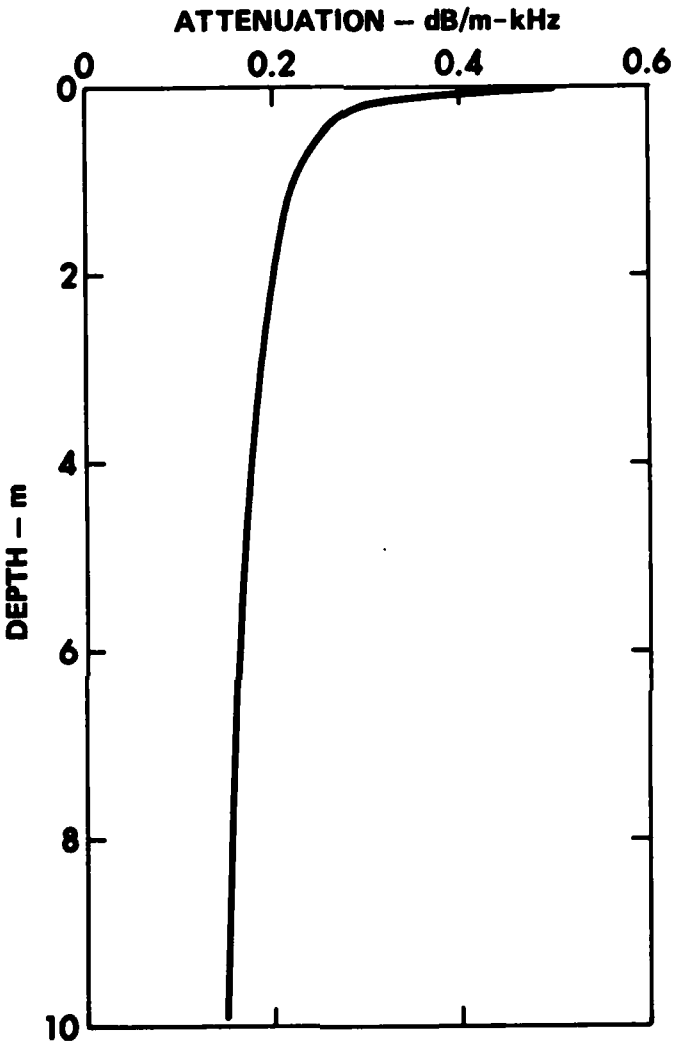

FIGURE II.3
COMPRESSIONAL WAVE ATTENUATION PROFILE FOR A SAND SEDIMENT

ARL:UT
AS-82-368-P
KCF-GA
3-30-82

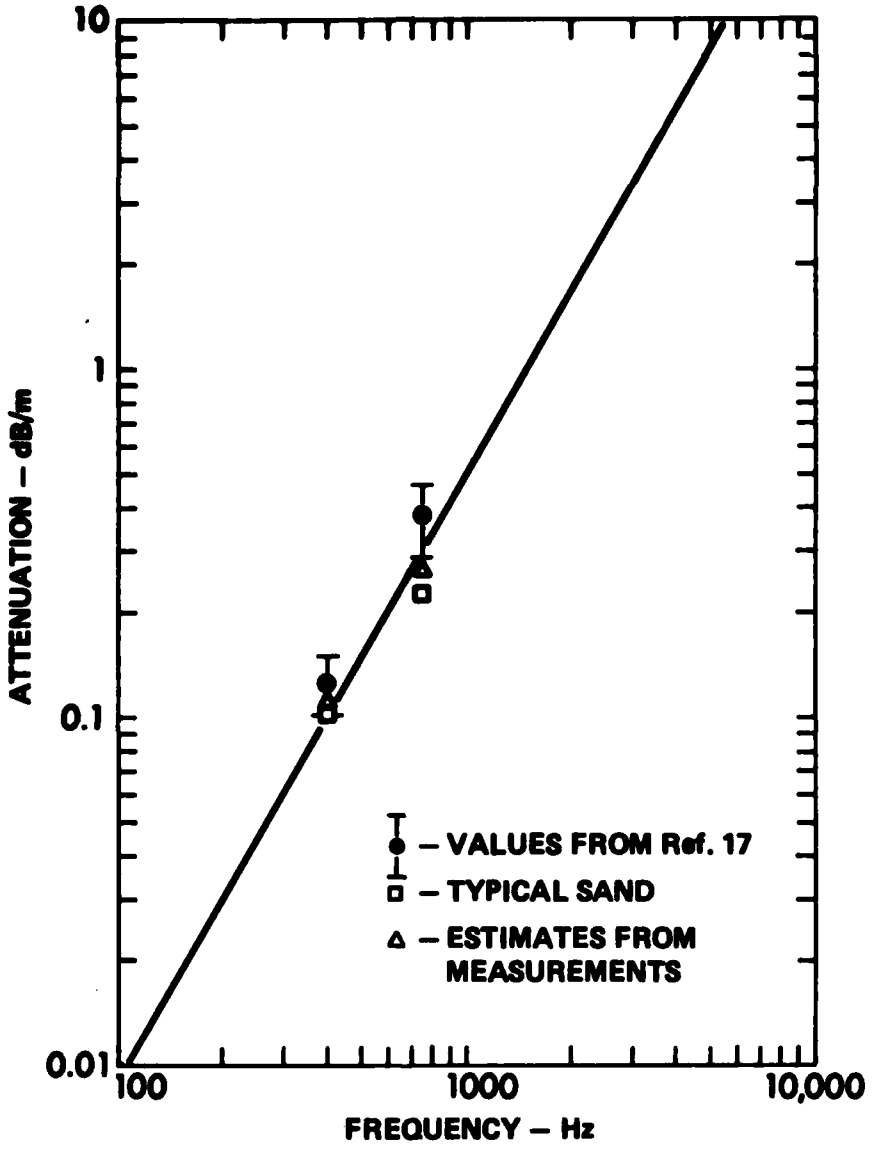

FIGURE II.4
COMPARISON OF CALCULATED ATTENUATIONS $\alpha'(f)$ FOR THE ATTENUATION PROFILE IN Fig. II.3 AND DATA FROM Ref. 17

ARL:UT
AS-82-359-P
KCF - GA
3 - 30 - 82

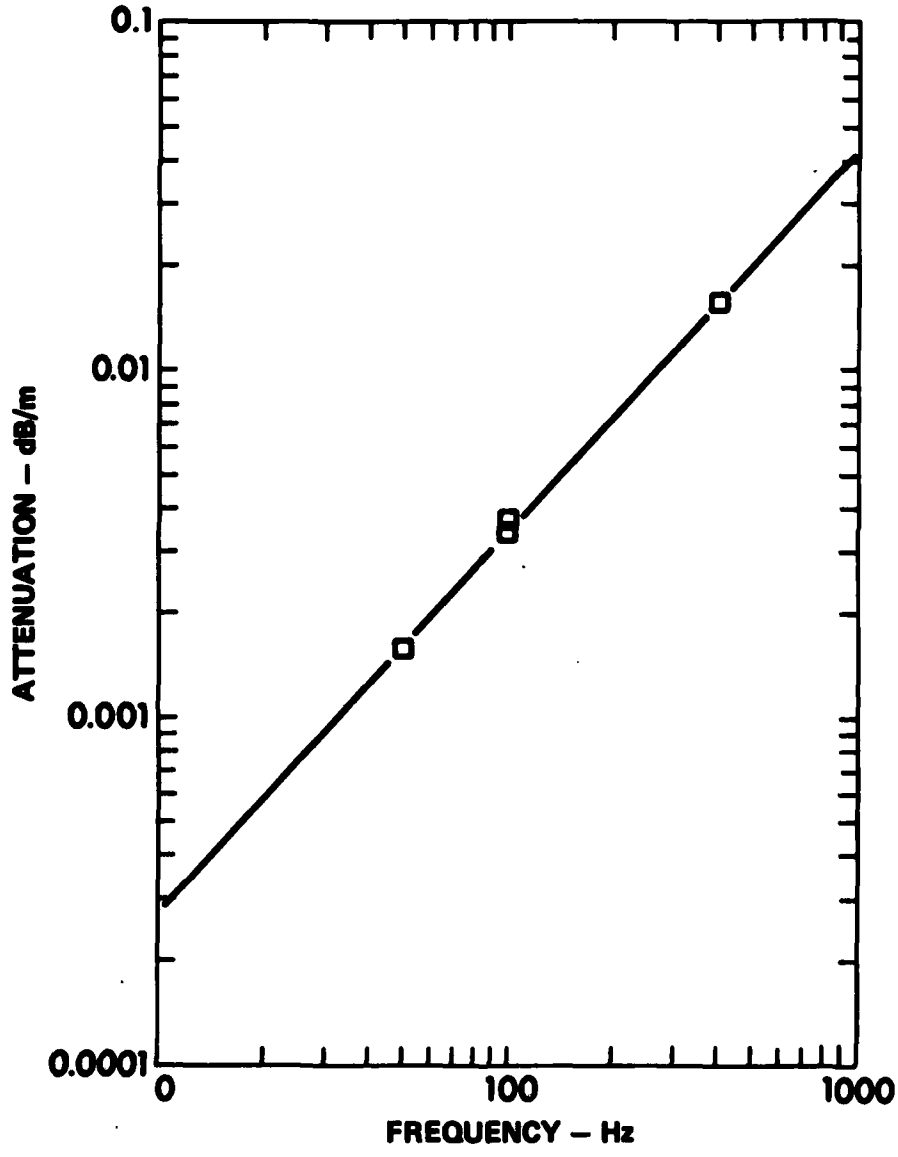

FIGURE II.5
COMPARISON OF CALCULATED DEPTH-CONSTANT ATTENUATIONS FOR THE MODIFIED VERSION OF PROFILE 1, Fig. II.1, AND RESULTS FROM Ref. 16

ARL:UT
AS-82-360-P
KCF - GA
3 - 30 - 82

CHAPTER III
ESTIMATING THE ATTENUATION PROFILE

The importance of the depth variations in the attenuation was brought out in the discussions presented in the preceding chapter. When acoustic propagation data are analyzed under the assumption that attenuation is invariant with depth, one can misinterpret the attenuation dependence on frequency or overemphasize the importance of other loss mechanisms. To avoid these pitfalls, the attenuation needs to be described and analyzed, not only as a function of frequency, but also as a function of depth. A method or procedure is needed which will estimate the attenuation depth profile within a measurement region.

A method can be devised for estimating the attenuation profile which will take advantage of variations in the shape of the low order normal modes as the frequency varies. These variations, combined with the frequency dependence of the sediment attenuation, result in the observed frequency dependence in the measured propagation loss. Estimates can be obtained without requiring direct in situ measurements of the sediment properties. The only measurements required are those generally taken during acoustic propagation experiments.

A. Input Parameters

The estimation technique requires propagation loss measurements and an environmental description. The environmental description includes the sound speed profile in both the water and sediment, the density of both the water and the sediment, and an estimate of the thickness of the sediment. Propagation loss measurements collected at multiple frequencies are affected by the

acoustic attenuation in the sediment and can be used to estimate the attenuation profile.

Sediment attenuation values are assigned to various depths based on characteristics of the normal modes to be discussed below. The calculations of the normal modes require input parameters defining the acoustic environment. The sound speed profiles in both the water and the sediment layers are the most important of these. The sound speed profiles enter into the calculation of the modes through Eq. II.6, and thus determine how much energy will penetrate into the bottom sediments. The sound speed in the sediment also enters into the determination of the mode attenuation term through Eq. II.9. Changes to the sound speed profile will result in changes in the calculated modes and in the calculated mode attenuation terms.

Propagation loss measured as a function of range is significantly influenced by the attenuation in the sediment. Information about the attenuation is contained within these measurements. The propagation loss has to be measured at several frequencies in order to estimate the attenuation profile. There is a sediment layer defined for each frequency, and therefore the depth resolution of the estimates is a function of the number of frequencies for which there are measurements.

B. Frequency Characteristics of the Normal Modes

There is one characteristic of the normal modes that is important to the procedure for estimating the attenuation profile in shallow water sediments. This characteristic will be referred to as the penetration depth of the mode.[30] This depth defines how much of the sediment affects the mode. This depth has also been called the hidden depth,[31] meaning that the sediment below this depth is hidden from the mode. For any specific sediment, this penetration depth is a function of frequency. As the frequency decreases, the penetration depth increases into the sediment. This frequency dependence can be

demonstrated by looking at the results obtained in a shallow water environment consisting of two isovelocity layers: c_1 is the sound speed in the water layer of thickness H, and c_2 is the sound speed of the sediment layer of semi-infinite thickness. This was the description used by Pekeris,[30] who noted the frequency dependence of the penetration depth. For this environment, the mode function in the sediment layers is described by decaying exponentials,

$$\psi_n(z) = D \exp\left[- (\kappa_n^2 - k^2)^{1/2} z \right], \qquad \text{III.1}$$

where z is depth, $k = \omega/c_2$, D is a constant satisfying the boundary conditions, κ_n is the eigenvalue, and ω = the angular frequency. κ_n approaches ω/c_1 at the higher frequencies and approaches ω/c_2 at the lower frequencies. κ_n is monotonic in ω between these two limits. As the frequency increases, the decay constant in Eq. III.1, $(\kappa_n^2 - k^2)^{1/2}$, increases, and the mode function decreases more rapidly with depth.

In Chapter II, the mode attenuation term was found to be

$$\delta_n = \frac{\omega}{\kappa_n I_n} \int \rho(z) \frac{\alpha(z)}{c(z)} \left|\psi_n(z)\right|^2 dz \quad , \qquad \text{II.9}$$

This equation shows that the influence of the attenuation within a sediment layer is dependent upon the integral across that layer of the eigenfunction squared. To understand the interaction between the mode and the sediment attenuation, consider a hypothetical attenuation profile defined by

$$\alpha(z) = a + g(z) \quad ,$$

with the mode function in the sediment given by Eq. III.1. The partial contribution to δ_n from the sediment at depths less than z is given by

$$d_n(z) = \left[1 - \left(1 + \frac{gz}{g + 2\tau a}\right) e^{-2\tau z}\right] \delta_n \quad , \qquad \text{III.2}$$

where $\tau=(\kappa_n^2-k^2)^{1/2}$. At a fixed z, as the frequency increases (increasing τ), the second term in Eq. III.2 decreases, and therefore the relative contribution increases. The shallower sediment layers will contribute more to the total mode attenuation at the higher frequencies while the deeper sediment layers will only contribute to the lower frequency attenuations.

When the sound speed in the sediment changes with depth, Eq. III.1 still approximates the low order mode functions within the sediment. The influence of the deeper sediments upon mode attenuation is therefore expected to increase with decreasing frequency. This can be demonstrated by looking at the first mode for two frequencies, 50 and 400 Hz, for more realistic environments. The first environment is 430 m of isovelocity water overlying 50 m of a clay sediment (Fig. III.1). The sediment sound speed is defined by an interface sound speed ratio of 1.0 at the water-sediment boundary, and by a sound speed gradient of 1.0 sec^{-1}. This is a nominal description for a clay sediment. Figure III.1 presents mode 1 at both 50 and 400 Hz for the environment described above. At 50 Hz the mode extends down through the sediment layer, while at 400 Hz an appreciable amplitude extends down only to 10 m. The influence of attenuation at depths below 10 m is expected to be greater at 50 Hz than at 400 Hz. Figure III.2 presents a more detailed look at the modes within the sediment. The dotted curves are the mode functions within the sediment normalized to a value of one at the sediment surface. The mode function at 50 Hz decreases more slowly than the one at 400 Hz, as suggested by Eq. III.1.

As was stated above, the mode attenuation coefficient involves the integral of the mode function squared. The solid curves in Fig. III.2 present the accumulative value for this integral as a function of depth into the sediment. These curves have been normalized so that the total integral has a value of one, and are related to Eq. III.2. At 400 Hz, 98% of this integral occurs above 10 m. At 50 Hz, however, only 55% of the integral has occurred within this 10 m.

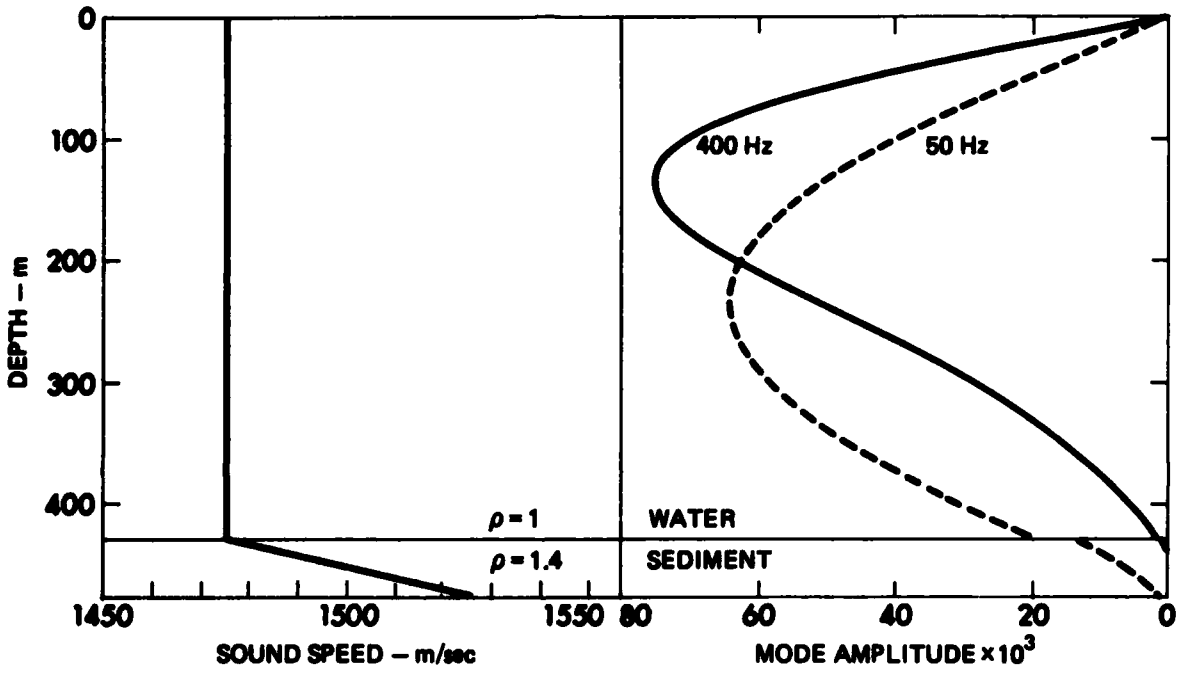

FIGURE III.1
ENVIRONMENTAL DESCRIPTION AND MODE 1 AT 50 Hz AND 400 Hz FOR A SHALLOW WATER AREA

ARL:UT
AS-82-1594
KCF-GA
10-6-82

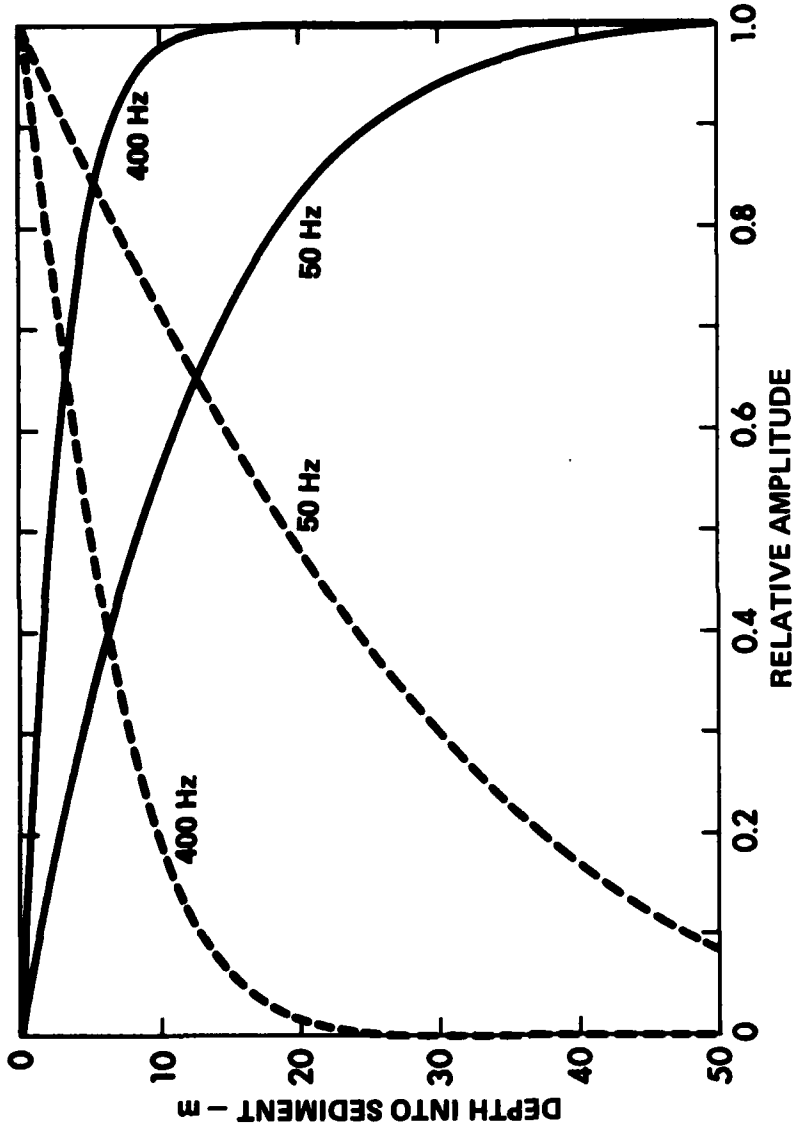

FIGURE III.2
DISTRIBUTION OF MODE QUANTITIES IN THE SEDIMENT FOR MODE 1 AT 50 Hz AND 400 Hz
(- - - - -) RELATIVE AMPLITUDE OF THE MODE FUNCTION,
(———) INTEGRAL OF MODE FUNCTION SQUARED
CLAY-SILT BOTTOM

ARL:UT
AS-81-1108
KCF - GA
8 - 21 - 81

The sediment attenuation in the first 10 m almost totally determines the mode attenuation coefficient at 400 Hz. Sediment attenuation values down to 40 m are important in the determination of the coefficient at 50 Hz, however.

A second environment to consider is 90 m of water overlying 30 m of a sand sediment. The sound speed profile in the water is downward refracting, and the sound speed profile in the sand follows descriptions given by Hamilton.[1] Figure III.3 presents the normalized mode function and mode function integral in the sediment for 50, 400, and 1600 Hz. From these figures, it is seen that the modes in this case have depth dependencies similar to those in the previous case. The higher frequencies only penetrate to shallowest depths. The lower frequencies penetrate the deeper sediments, although the depths of penetration are less than those seen in Fig. III.2. The mode attenuation for the highest frequencies are determined by just the surface sediments, and as the frequencies decrease more of the sediment enters into this determination.

C. Estimating the Attenuation Profile

The relationship between the frequency and the penetration depth presented above suggests a method for estimating the sediment attenuation profile. By examining the frequency dependence of the propagation loss in terms of the penetration depths, one can estimate an attenuation profile.

An estimation procedure was developed around the relationship between frequency and penetration depth. It uses propagation loss measured at multiple frequencies and the linear frequency dependence of the attenuation in the sediment. The sediment can be divided into layers according to the penetration depths for the frequencies available in the measurements. Estimates of the sediment attenuation within each

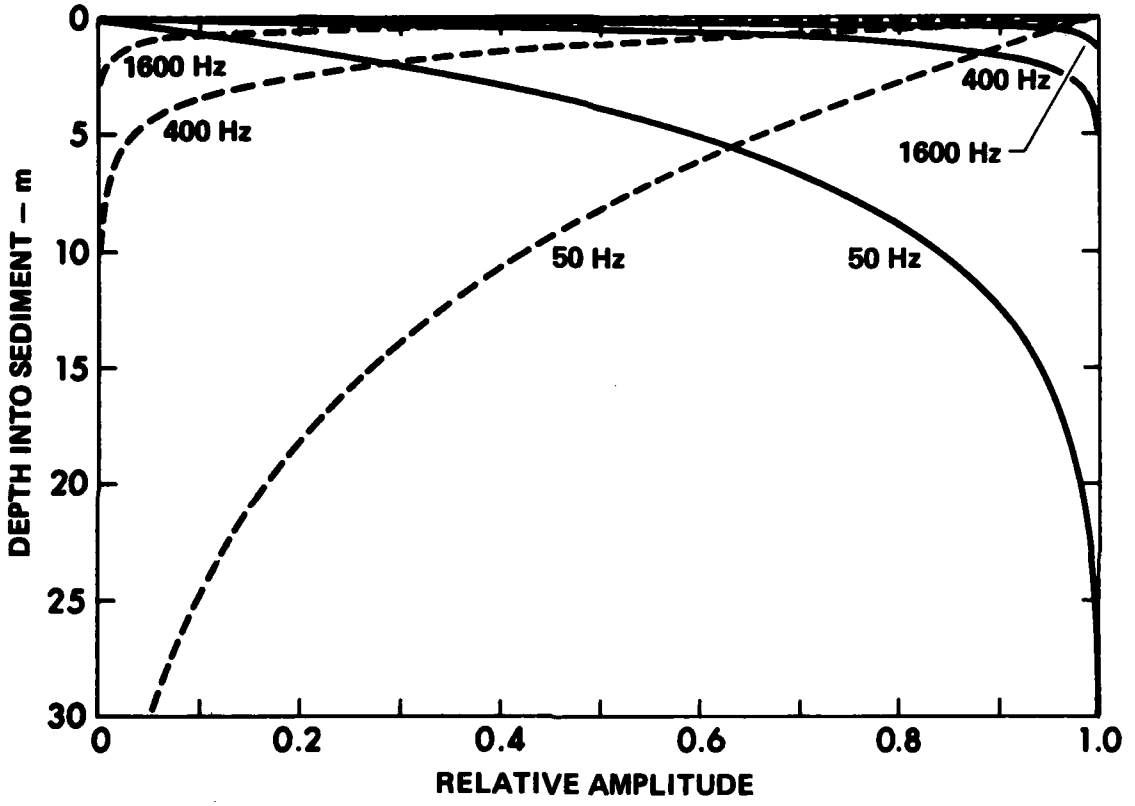

FIGURE III.3
DISTRIBUTION OF MODE QUANTITIES IN THE SEDIMENT FOR MODE 1 AT 50, 400, AND 1600 Hz
(- - - - -) RELATIVE AMPLITUDE
(———) INTEGRAL OF MODE FUNCTION SQUARED
SANDY BOTTOM

ARL:UT
AS-82-1132
KCF - GA
7 - 9 - 82

layer are determined from the propagation loss measurements at the frequency corresponding to that layer.

The procedure is divided into two parts, as illustrated in Fig. III.4. The first step is to define layer depths and the second is to determine the attenuation values in each layer. Propagation beyond a few water depths involves only the lowest order modes. Therefore, for each frequency one sediment layer will be defined by considering only mode 1. The integral of the mode function squared is computed as a function of depth, as presented in Figs. III.2 and III.3. A layer depth can now be defined as the depth at which this integral exceeds a specified fraction of the integral computed across the entire sediment column. For example, using 80% of the total integral, layer depths of 4.7 m and 18 m are obtained for the modes presented in Fig. III.2, and depths of 0.5 m, 1.2 m, and 8.6 m for Fig. III.3. If there are data at n frequencies available, there will be n sediment layers defined. The last layer, instead of extending down to the 80% depth of the lowest frequency, would extend down to the bottom of the sediment column.

With the layer depths defined, the attenuation values can be estimated by comparing the measured propagation losses to the calculated losses. The estimates of sediment attenuation $\hat{\alpha}$ are initially assumed to be the same in all the sediment layers. Then, beginning with the highest frequency of interest for which there are measurements, 800 Hz in Fig. III.4, the sediment attenuation $\hat{\alpha}$ is varied to minimize the difference between the measured and calculated results. The calculated propagation losses are computed using the incoherent mode sum given in Eq. II.5. The value thus obtained, $\hat{\alpha}_1$, is assigned to the initial sediment layer and varies linearly with frequency. The model/data comparisons are now conducted for the next lower frequency of interest. The attenuation in the sediment below the first layer is again assumed to be constant between these deeper layers and is varied to minimize the propagation loss differences at this frequency. The attenuation value obtained, $\hat{\alpha}_2$, is assigned to the second layer, again varying linearly with frequency. The procedure is now repeated for the third

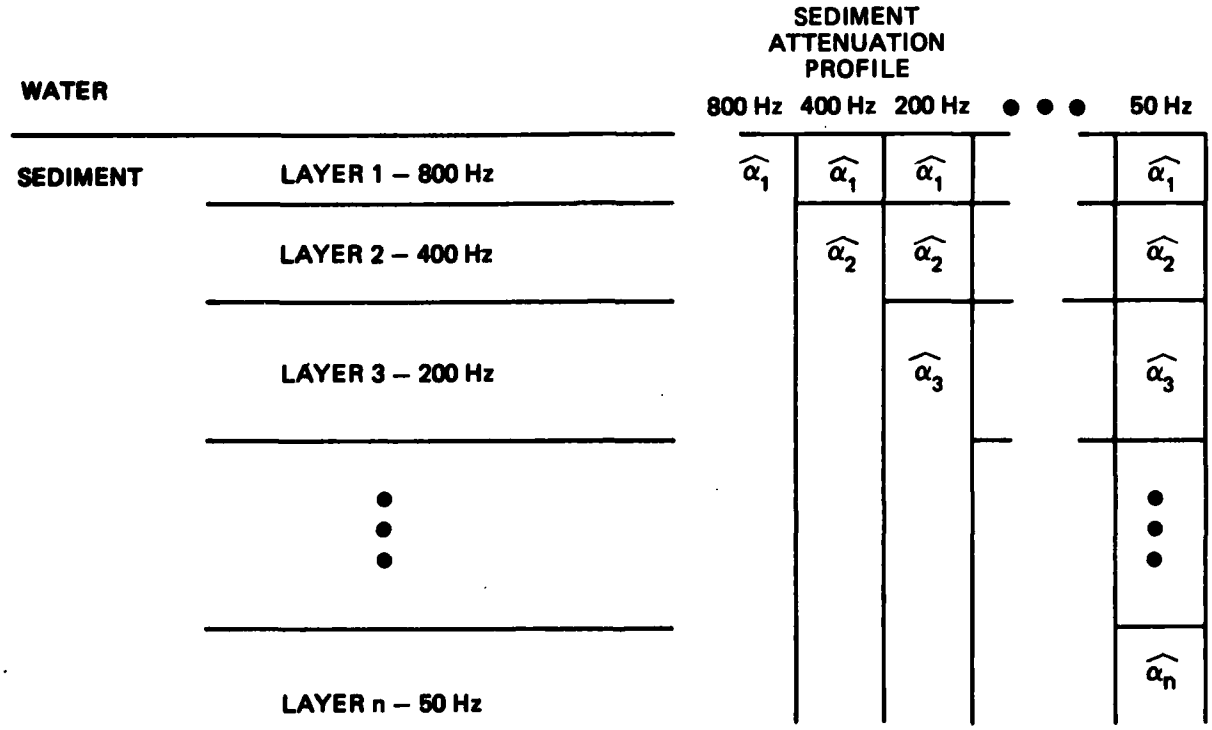

FIGURE III.4
ATTENUATION PROFILE GENERATED BY FREQUENCY CONSIDERATIONS

ARL:UT
AS-82-1220
KCF - GA
8 - 5 - 82
REV 10-28-82

highest frequency, and is continued until all available frequencies have been considered. The final result is an attenuation profile, described by n layers of constant attenuation and a linear frequency dependence.

Calculated propagation losses versus range were used to simulate measured values based on a hypothetical environment. In this way, the actual attenuation profile was known, and a comparison between actual and estimated profiles can be performed. The environment presented in Fig. III.1 along with the two attenuation profiles represented by the solid curves in Fig. III.5 were used to compute propagation losses. Propagation losses were calculated as a function of range at frequencies of 50, 100, 200, 400, and 800 Hz using the computer normal mode model NEMESIS.[28,29] These calculated values of propagation loss were then used as if they were data in the estimation procedure outlined in Fig. III.4. The estimates were based on the $\psi_n(z)$'s and κ_n's obtained for the propagation loss calculations.

The estimated attenuation profiles are presented in Fig. III.5 as dashed lines. For these estimates, the sediment layer depths were defined by 80% of the total mode square integral. In both cases the five-layer profile approximates the input profile, with the major difference occurring in the first layer. The first layer as attenuations are biased slightly towards the deeper layer values. Figure III.6 presents the propagation loss comparisons for the actual and the estimated profiles. The maximum error between any two corresponding curves is less than 1 dB and the maximum mean square error for any one frequency was 0.2 dB.

The comparison just presented was an ideal case. The environment was known exactly and the propagation loss inputs were exact and not corrupted by noise. For actual measurements, the environmental description will generally be composed of several measured parameters, such as the water sound speed profile, while the remaining parameters must be inferred from indirect methods. The sediment sound speeds and densities are inferred from the sediment type and subbottom profiling.

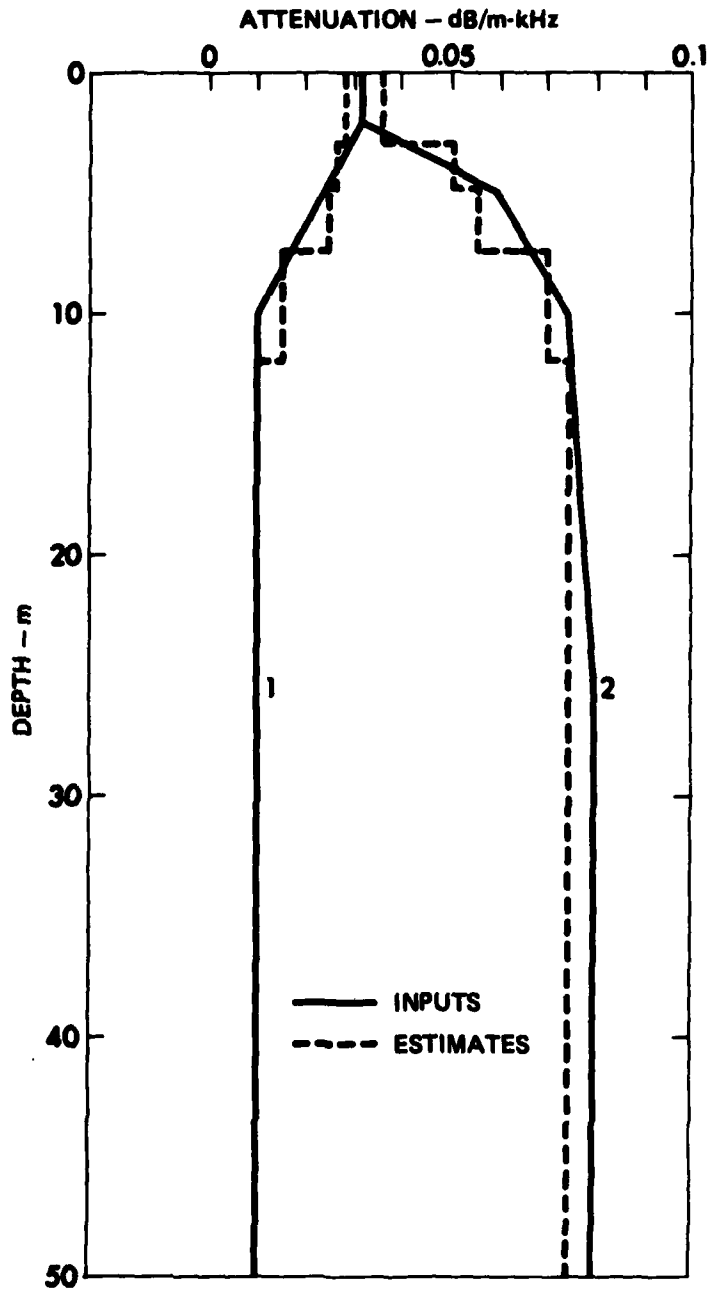

FIGURE III.6
COMPARISON BETWEEN INPUT AND ESTIMATED ATTENUATION PROFILES

ARL:UT
AS-82-1595
KCF-GA
10-6-82

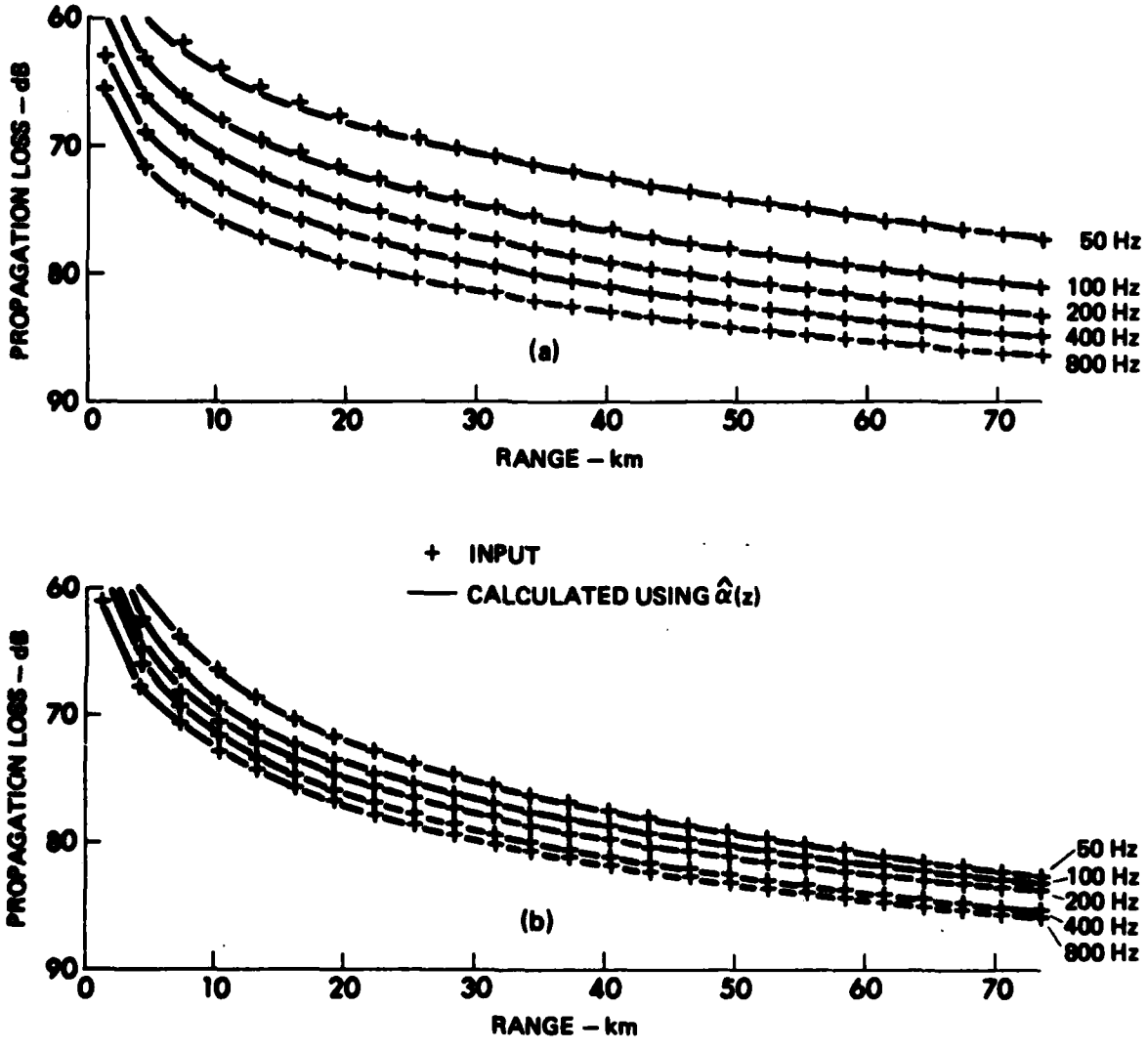

FIGURE III.6
PROPAGATION LOSS COMPARISON BETWEEN INPUT AND CALCULATION BASED ON ESTIMATED ATTENUATION PROFILE

(a) PROFILE 1 FIGURE
(b) PROFILE 2 FIGURE

ARL:UT
AS-82-1566
KCF - GA
10 - 6 - 82

CHAPTER IV
ATTENUATION PROFILES IN EXAMPLE SHALLOW WATER REGIONS

Chapter III presented a procedure for estimating the attenuation profile in shallow water regions which is based on acoustic propagation measurements. The procedure will be applied to measured propagation loss data collected in three regions. Data collected in each region provided the information necessary to obtain the estimates. Acoustic propagation measurements were obtained using explosive sources, that generated broadband signals. This provided propagation loss measurements at multiple frequencies, as required. There was also sufficient information collected about the environments to allow the sound speed profiles in both the water and sediment layers to be described. The normal modes could therefore be calculated for each region.

A. Environmental Descriptions

Figures IV.1-IV.3 present the measured propagation loss and the bathymetry along the source tracks for three measurement sites. These three sites provided a variety of environmental conditions: three different water depths, two sediment types, and two water sound speed profiles.

Site 1, Fig. IV.1, lies within a sedimentary basin. The sediment in this region of the basin has been classified as clay based on seismic refraction profiling and sediment coring samples. The sound speed profile was defined by a water-sediment sound speed ratio of 1, a gradient of 1 sec^{-1}, and a thickness of 50 m. The water depth at this site was 430 m and the sound speed profile was described as isovelocity (Fig. III.1).

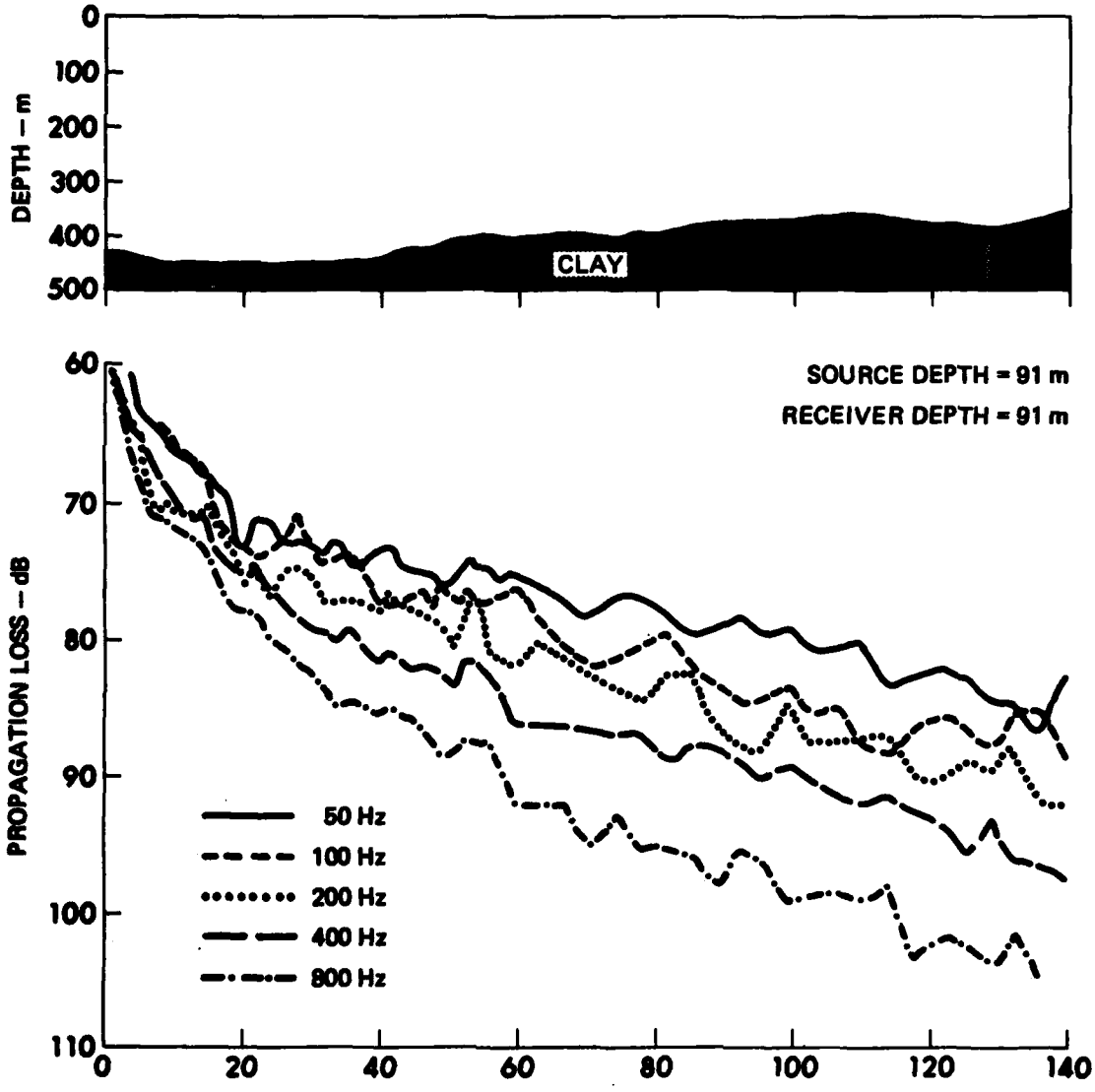

FIGURE IV.1
BATHYMETRY AND MEASURED PROPAGATION LOSS FOR SITE 1

ARL:UT
AS-82-1597
KCF-GA
10-6-82

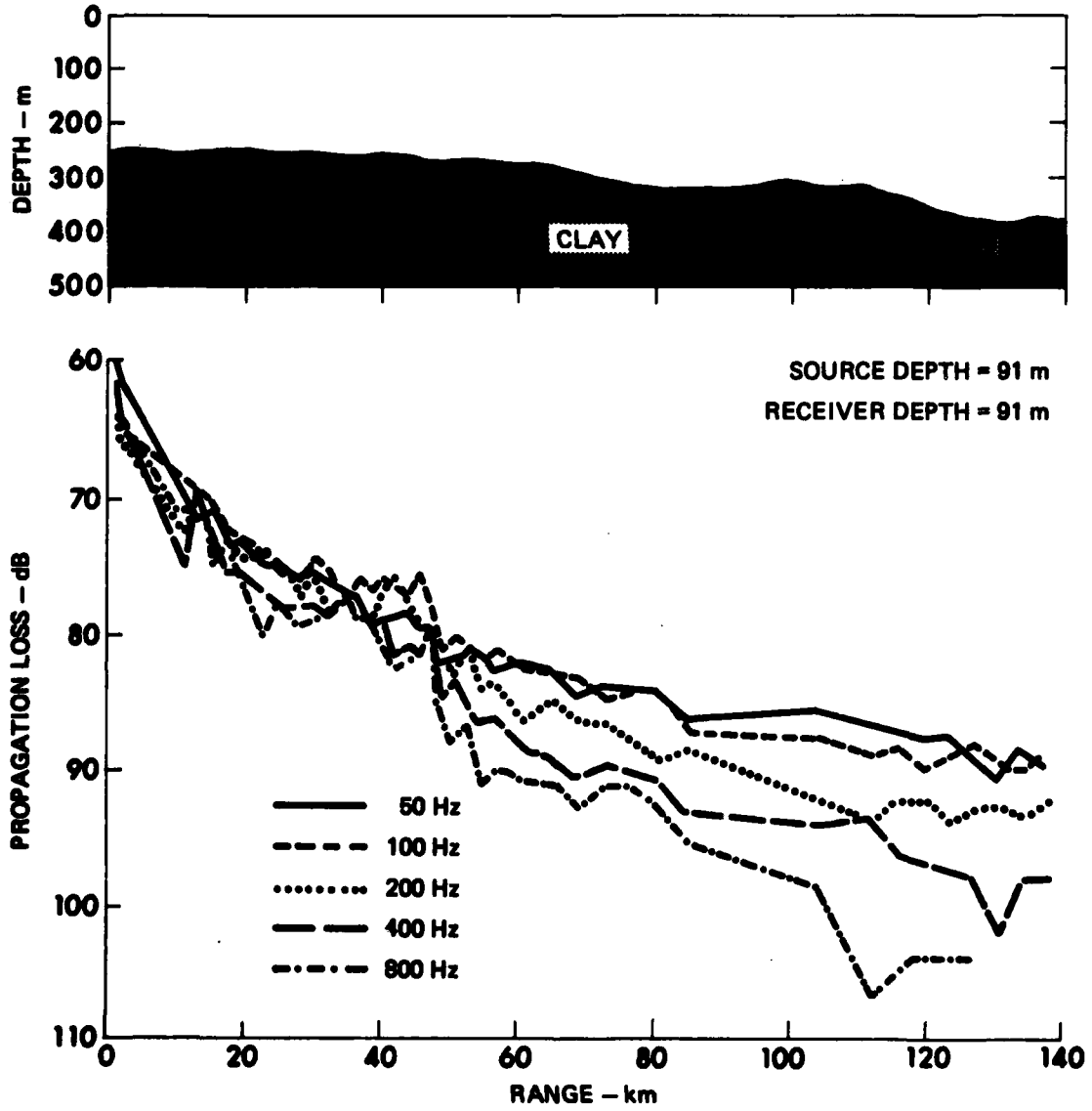

FIGURE IV.2
BATHYMETRY AND MEASURED PROPAGATION LOSS FOR SITE 2

ARL:UT
AS-82-1598
KCF - GA
10 - 6 - 82

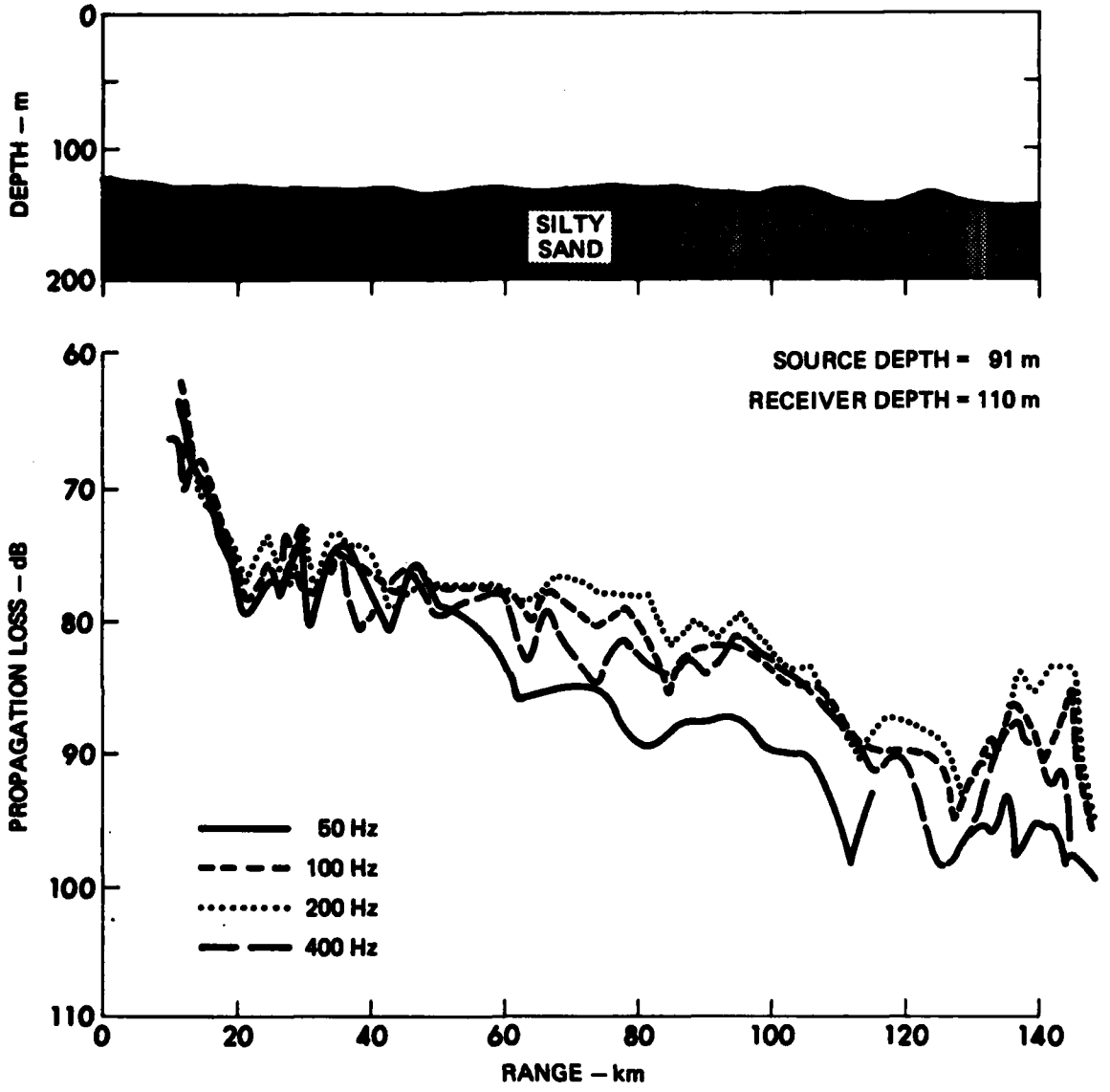

FIGURE IV.3
BATHYMETRY AND MEASURED PROPAGATION LOSS FOR SITE 3

ARL:UT
AS-82-1599
KCF - GA
10 - 6 - 82

Site 2, in Fig. IV.2, was located 250 km from site 1 on a bathymetric high outside the sedimentary basin at site 1. The water depth was 250 m and again the sound speed profile was isovelocity. Based on seismic profiling conducted in this area, the sediment at this site was assumed to be 50 m of clay with the same description as site 1. The attenuation in the sediment at this site, however, was not expected to be the same as at site 1.

Site 3, Fig. IV.3, was located on the continental shelf in 120 m of water. The water sound speed profile at this site was downward refracting, sound speed decreasing with depth. Sediment coring samples and seismic refraction profiling indicated the sediment type was silty sand. Within the first meter of sediment, the sound speed increased to 1670 m. The sound speed gradient decreased with depth throughout the 30 m of sediment.

B. Measured Propagation Loss

Figures IV.1-3 also present the propagation losses versus range for each site. The sources were detonated at a depth of 91 m for all three sites. The receiver depths were 91 m at sites 1 and 2, and 75 m at site 3.

The propagation losses to all three sites were relatively low. The losses at most frequencies did not exceed 95 dB at sites 1 and 2, or 90 dB at site 3, even out to ranges of 140 km.

At site 1 the measured propagation losses in the range interval 0-80 km was used to estimate the attenuation profile. The selection of this range interval was based on the bathymetry. Beyond 80 km, there was a decrease in water depth. To avoid the effects of change in water depth, the analysis was confined to the first 80 km.

At site 2, Fig. IV.2, the propagation losses show a change in the range dependence at a range of approximately 55 km. This change

correlates with a known change in the sediment, and therefore only ranges less than 55 km were used in the analysis. Within this range interval the propagation exhibited little dependence on frequency.

At site 3 there is no obvious change in the range dependence of propagation as seen at site 2. As at site 1, there was a change in water depth. The depth changed from 120 m at site 3 to 160 m at the end of the source track. The analysis was limited to the first 100 km to avoid possible effects due to the changing water depth.

C. Attenuation Profiles

The attenuation profiles were estimated for each of the three sites, based on the data presented in the last two sections. The estimated attenuation values were all within the ranges expected for the sediment type found at the measurement sites. The depth dependence of each profile also agreed with previously reported measurements.

Figure II.1 presented the attenuation profiles estimated for sites 1 (curve 1) and 2 (curve 2). The decrease in attenuation at site 1 was needed to account for the lower losses at the lower frequencies. The increase in attenuation with depth at site 2 was needed to account for the near frequency independent nature of the propagation loss. The differences between these two profiles indicate the variability in the attenuation values for clay type sediments.[9] Data compiled by Hamilton[1,9] had indicated that attenuation could either increase or decrease with increasing depth.

A comparison between the data and the final calculations at site 1 showed that the calculated losses generally were within 3 dB of the measurements. The comparisons at 50 Hz and 400 Hz are shown in Fig. IV.4. Comparisons at the other frequencies presented similar results. The rms differences, calculated at each frequency, varied from 2.3 dB at 400 Hz to 1.6 dB at 100 Hz.

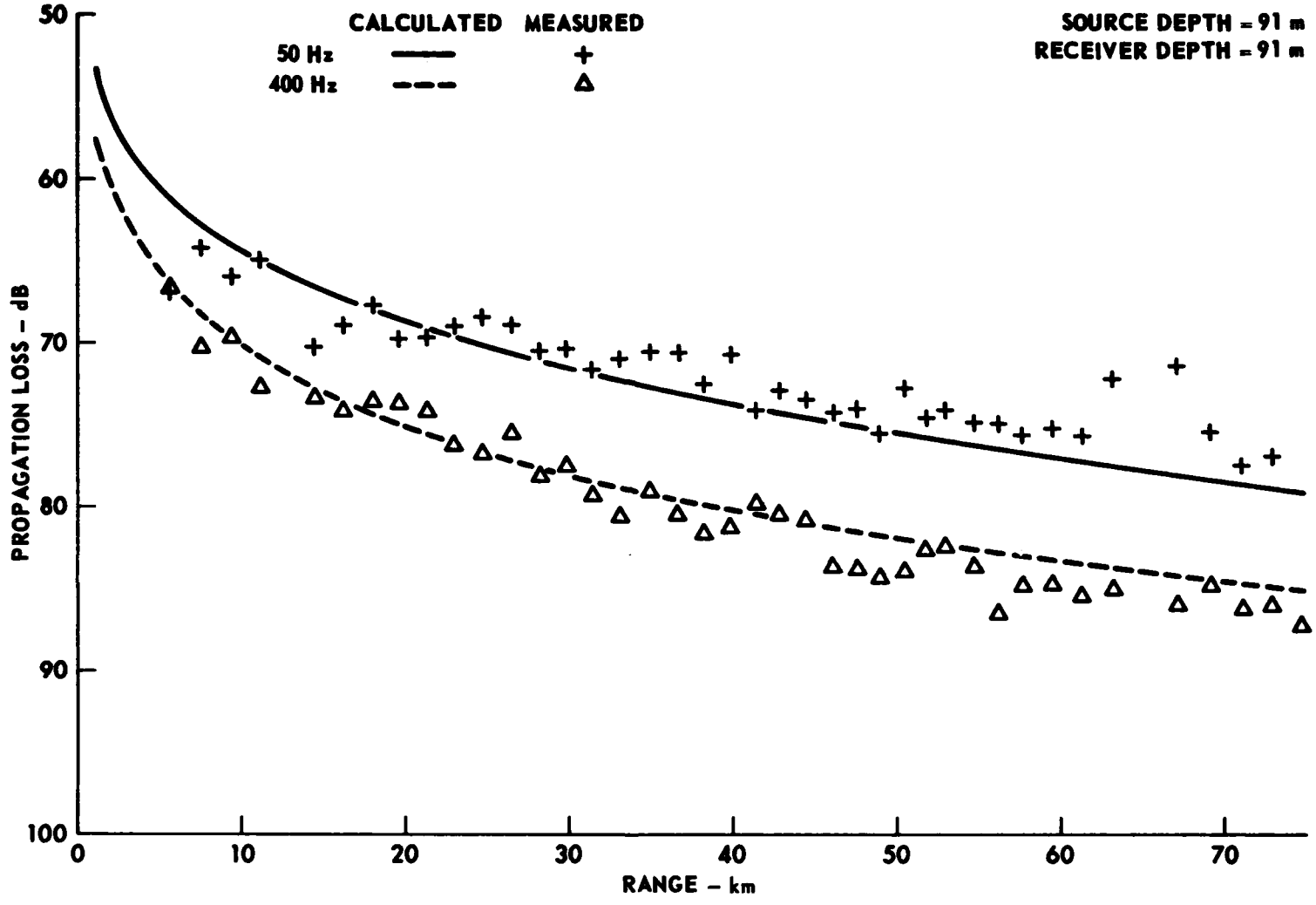

FIGURE IV.4
(U) COMPARISON OF CALCULATED AND MEASURED PROPAGATION LOSS AT SITE 1

ARL-UT
AS-80-562
KCF-GA
1-15-80

Comparisons of the final calculations and the measurements at site 2 were similar to those found at site 1. The calculations for this site were also generally within 3 dB of the measurements with the rms differences varying from 1.7 dB at 400 Hz to 1.4 dB at 50 Hz. Figure IV.5 presents the comparisons at 50 Hz and 400 Hz. Comparisons at other frequencies were similar, with the curves lying between those at 50 and 400 Hz.

For both sites 1 and 2, where the sediments were clay, the attenuation values were in the lower range of values expected for clays. These estimates varied from 0.01 up to 0.08 dB/m-kHz. Although the attenuation is generally expected to increase with depth,[9] the fact that at site 1 the profile decreases with depth is not a point of contention. The expected increase is based on a compilation of reported results within the first 400-500 m. The slight decrease in attenuation within the first 50 m of sediment is not a significant deviation from a trend seen in such a diversified set of measurements.

The estimated profile obtained for the sand sediment was also in agreement with the nominal profile[9] (Fig. IV.6). The attenuation varied from 0.28 to 0.6 dB/m-kHz, which is in the middle of the range for sands. The attenuation decreased with increasing depth. This was similar to the typical sand profile presented earlier in Fig. II.3.

The comparisons between calculated and measured propagation losses at site 3 were similar to those found at sites 1 and 2, Fig. IV.7. The calculations were generally within 3 dB of the measurements and the rms differences varied from 2.8 dB at 400 Hz to 3.5 dB at 50 Hz. The larger rms errors at this site were probably due to an increase in the point to point variation of the measurements.

All three profiles estimated by the procedure in Chapter III were in general agreement with measurements reported by Hamilton.[9] The rms differences in the calculated propagation losses were significantly larger than those found in the test case at the end of

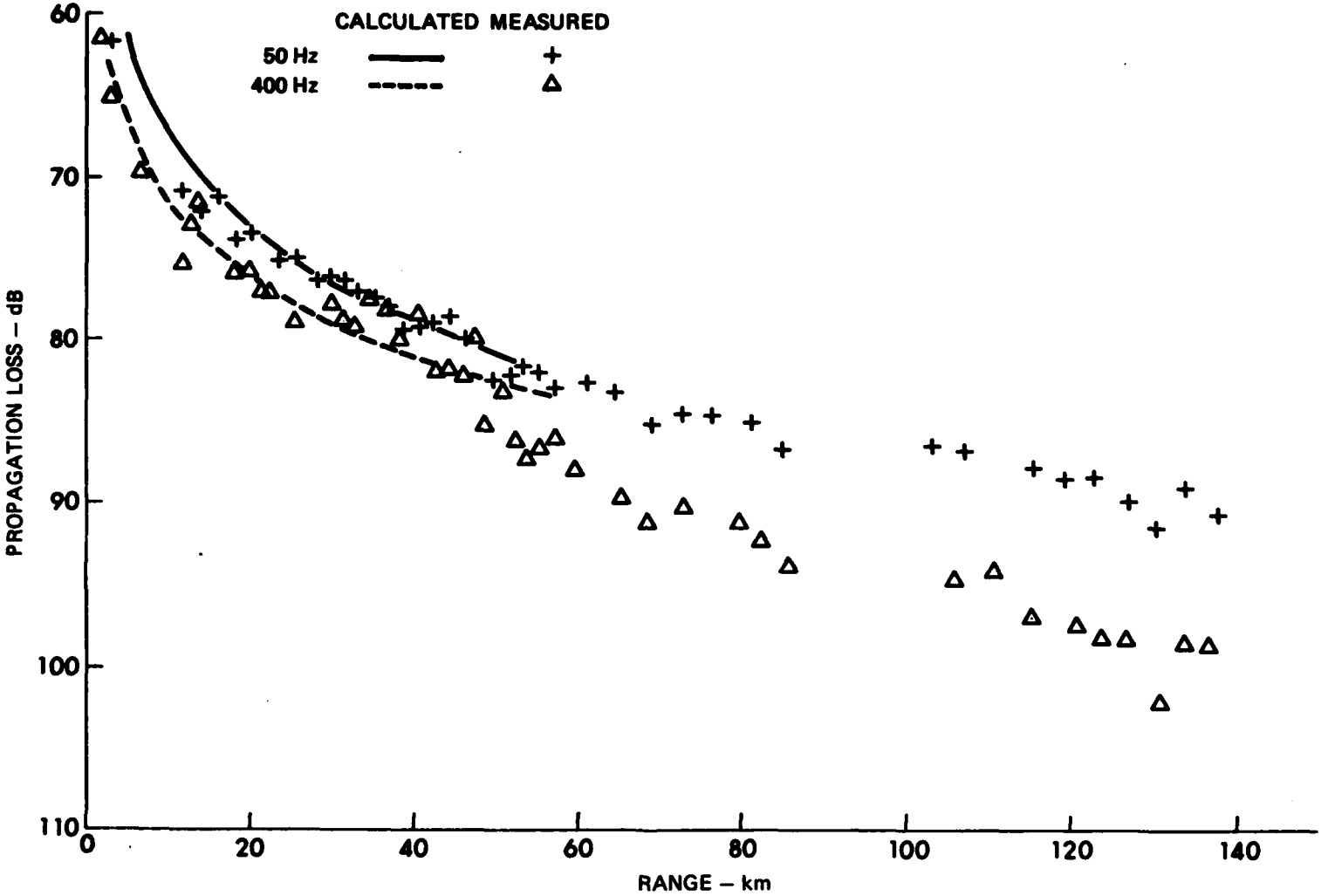

FIGURE IV.5
COMPARISON OF CALCULATED AND MEASURED PROPAGATION LOSS AT SITE 2

ARL:UT
AS-82-1706
KCF-GA
10-28-82

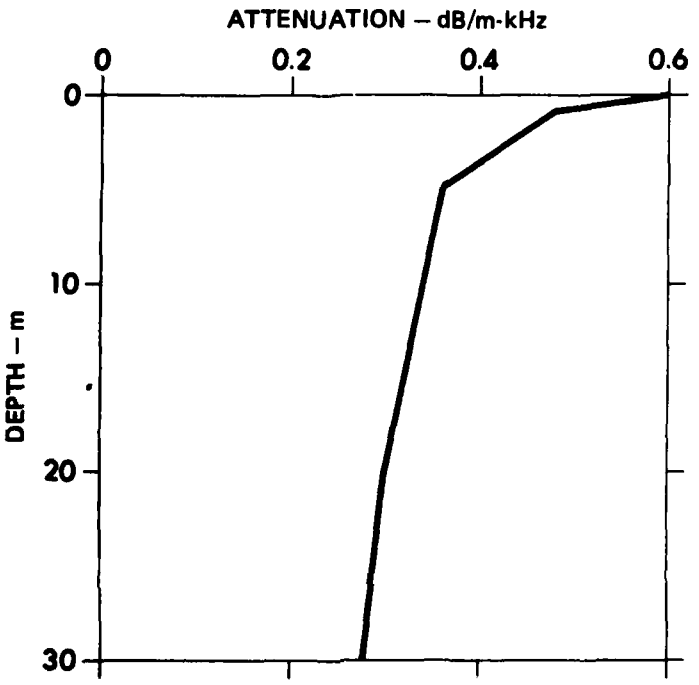

FIGURE IV.6
ESTIMATED ATTENUATION PROFILE
FOR SITE 3

ARL:UT
AS-82-1600
KCF - GA
10 - 6 - 82

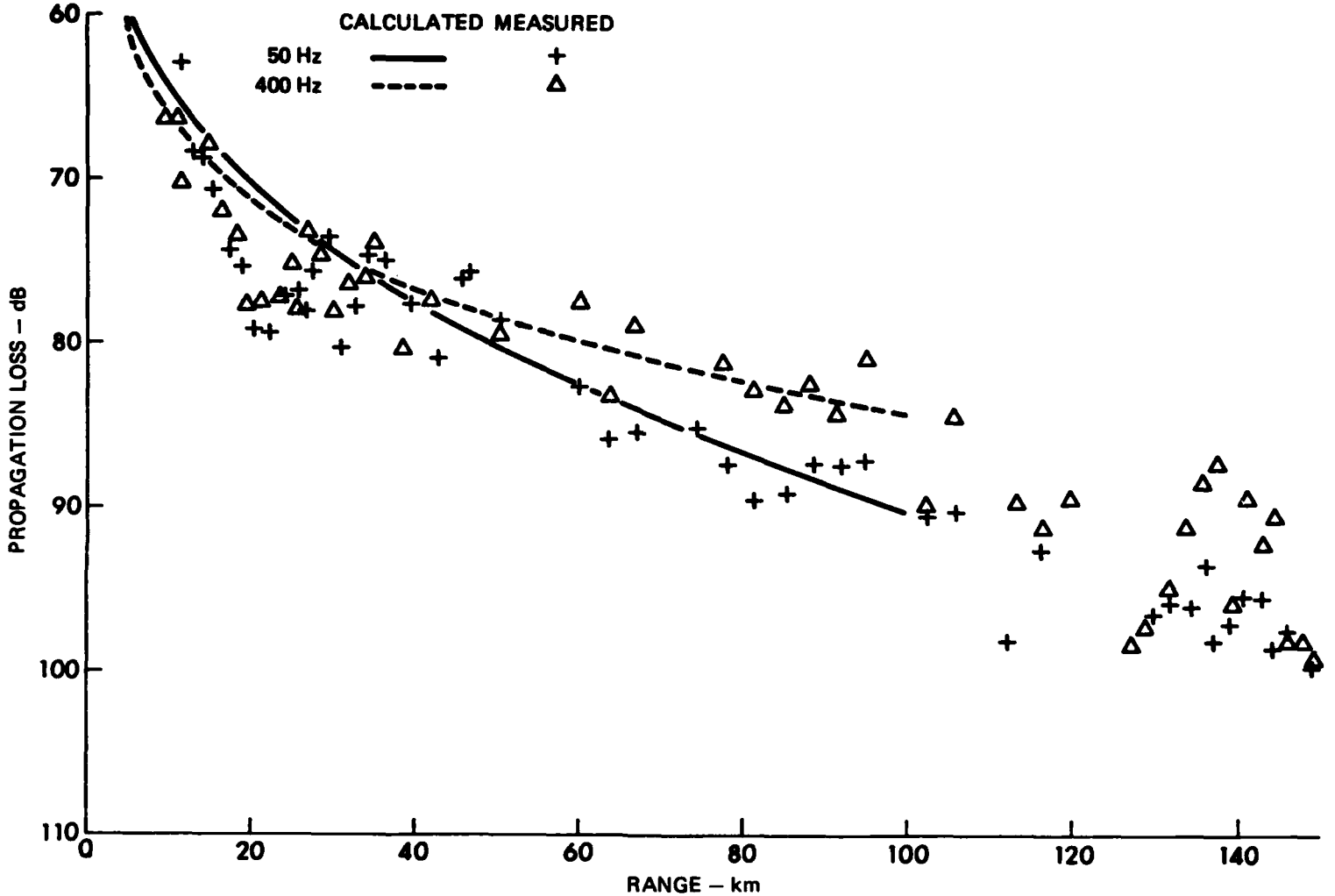

FIGURE IV.7
COMPARISON OF CALCULATED AND MEASURED PROPAGATION LOSS AT SITE 3

ARL:UT
AS-82-1707
KCF - GA
10-28-82

Chapter III, 2 dB compared to 0.2 dB. There are several possible sources of these errors. The estimated profiles were based on sediment sound speeds derived strictly from the sediment type. The measured propagation loss did not strictly conform to the incoherent summation of the modes assumed by the calculations. The data displayed point to point variations resulting from possible experimental errors, variations in the noise, and variations in the actual propagation losses. Each of these deviations lead to the increased differences found between the calculated and measured propagation losses.

D. Conclusions and Recommendations

The examples above show that the attenuation profiles in sediments of the bottoms of shallow ocean regions can be estimated using propagation loss measurements. The estimation technique in Chapter III is based on normal mode theory and the fact that propagation beyond a few water depths involves only the lower order modes. The depth of penetration of these modes are frequency dependent. The low frequencies penetrate deeper than the higher frequencies. The frequency-depth of penetration relationship and the frequency dependence of the measured propagation loss are used to obtain the attenuation profile estimates.

The estimated attenuation profiles discussed in this chapter (as shown in Figs. II.1 and III.4), agree with the characteristics of attenuation profiles measured in situ and in the laboratories,[1] discussed in Chapter II. The agreements are between the estimates and measurements made in similar sediment types. The estimates in clays are in the range 0.01-0.1 dB/m-kHz, typical of clays. In sand the estimates are in the range 0.2-0.9 and decrease with depth, which is typical of attenuation in sand.

The agreements found between these attenuation profiles and laboratory and in situ measurements is encouraging. However, there are several recommendations that can improve the estimation procedure. In the examples presented above, only a limited portion of the data sets

were used in the estimation of attenuation. Estimation beyond some range was eliminated because of a significant change in the environment. It should be possible to expand and modify the present technique to use the longer range data in obtaining a range dependent attenuation estimate. Besides extending the usefulness of the propagation data, this would provide a more complete description of a measurement region.

Another step that is needed is an error analysis of the attenuation estimates. The calculated incoherent propagation loss curves are smooth monotonic functions of range. The measured losses, however, contain variations about a general trend of increasing loss with increasing range. These variations result from interference between modes, inhomogeneities in the environment, and experimental error. These variations in the measured losses introduce uncertainties in the attenuation estimates. More sophisticated calculations of propagation loss could account for the interference between modes. The variations due to the inhomogeneities and measurement errors, however, will still lead to uncertainties in the estimates. At the moment, the estimation technique provides an attenuation profile, but does not indicate what the confidence limits or the error bounds are.

The difficulty in setting the confidence limits is deciding what those limits mean and how they should be determined. There will be errors associated with attenuation values assigned to each sediment. There will also be errors associated with the fact that the sediment is described by a limited number of layers and not as a continuum.

The estimation technique needs to be applied to a larger number of data sets. By examining more and more data sets, the actual need for range dependent estimates can be determined. More data sets may also indicate how confidence limits can be defined.

REFERENCES

1. E. L. Hamilton, "Geoacoustic Modeling of the Sea Floor," J. Acoust. Soc. Am. 68, 1313-1340 (1980).

2. L. M. Brekhovskikh, Waves in Layered Media (Academic Press, New York, 1960).

3. I. Tolstoy and C. S. Clay, Ocean Acoustics Theory and Experiment in Underwater Sound (McGraw-Hill Book Co., Inc., New York, 1966).

4. C. B. Officer, Introduction to the Theory of Sound Transmission with Application to the Ocean (McGraw-Hill Book Co., Inc., New York, 1958).

5. S. K. Mitchell and K. C. Focke, "New Measurements of Compressional Wave Attenuation in Deep Ocean Sediments," J. Acoust. Soc. Am. 67, 1582-1589, 1980).

6. K. E. Hawker, A. L. Anderson, K. C. Focke, and T. L. Foreman, "Initial Phase of a Study of Bottom Interaction of Low Frequency Underwater Sound," Applied Research Laboratories Technical Report No. 76-14 (ARL-TR-76-14), Applied Research Laboratories, The University of Texas at Austin, April 1976.

7. T. Akal, "Sea Floor Effects on Shallow-Water Acoustic Propagation," in Bottom-Interacting Ocean Acoustics, edited by W. A. Kuperman and F. B. Jensen (Plenum Press, New York, 1980), pp. 557-575.

8. S. K. Mitchell, N. R. Bedford, and G. E. Ellis, "Multipath Analysis of Explosive Source Signals in the Ocean," J. Acoust. Soc. Am. 67, 1590-1597 (1980).

9. E. L. Hamilton, "Sound Attenuation as a Function of Depth in the Sea Floor," J. Acoust. Soc. Am. 59, 528-537 (1976).

10. Y. P. Neprochnov, "Seismic Studies of the Crustal Structure beneath the Seas and Oceans," Oceanology 11, 709-715 (1971).

11. R. S. Jacobsen, G. G. Shor, Jr., and L. M. Dorman, "Linear Inversion of Body Wave Data, Part III: Attenuation versus Depth Using Spectral Ratios," Geophysics 46, 152-162 (1981).

12. A. N. Hunter, R. Legge, and E. Matsukawa, "Measurements of Acoustic Attenuation and Velocity in Sand," Acustica 11, 26-31 (1961).

13. R. D. Stoll, "Acoustic Waves in Ocean Sediments," Geophysics 42, 715-725 (1977).

14. M. A. Biot, "Theory of Propagation of Elastic Waves in a Fluid-Saturated Porous Solid, I. Low-Frequency Range," J. Acoust. Soc. Am. 28, 168-178 (1956).

15. R. D. Stoll and G. M. Bryan, "Wave Attenuation in Saturated Sediments," J. Acoust. Soc. Am. 47, 1440-1447 (1970).

16. L. A. Rubano, "Acoustic Propagation in Shallow Water over a Low-Velocity Bottom," J. Acoust. Soc. Am. 67, 1608-1613 (1980).

17. F. Ingenito, "Measurements of Mode Attenuation Coefficients in Shallow Water," J. Acoust. Soc. Am. 53, 858-863 (1973).

18. J. H. Beebe, S. T. McDaniel, and L. A. Rubano, "Shallow-Water Transmission Loss Prediction Using the Biot Sediment Model," J. Acoust. Soc. Am. 71, 1417-1426 (1982).

19. J. M. Hovem, "Attenuation of Sound in Marine Sediments," in Bottom-Interacting Ocean Acoustics, edited by W. A. Kuperman and F. B. Jensen (Plenum Press, New York, 1980), pp. 1-13.

20. A. Aubell, "Some Results of Computations of Transmission Loss Based on an Acoustic Propagation Model," in Proceedings No. 14 of Sound Propagation in Shallow Water Conference, SACLANTCEN, edited by O. F. Hastrup and O. V. Olesen, November 1974, pp. 112-128.

21. H. P. Bucker, "Normal-Mode Sound Propagation in Shallow Water," J. Acoust. Soc. Am. 36, 251-258 (1964).

22. C. T. Tindle and G. E. J. Bold, "Improve Ray Calculations in Shallow Water," J. Acoust. Soc. Am. 70, 813-819 (1981).

23. D. V. Bartorsky and L. B. Felsen, "Ray-Optical Calculation of Modes Excited by Sources and Scatterers in a Weakly Inhomogeneous Duct," Radio Science 6, 911-923 (1971).

24. L. I. Schiff, Quantum Mechanics (McGraw-Hill Book Co., Inc., New York, 1949).

25. R. A. Koch, C. Penland, P. J. Vidmar, and K. E. Hawker, "On the Calculation of Normal Mode Group Velocity and Attenuation," submitted to the Journal of the Acoustical Society of America, July 1982.

26. E. T. Kornhauser and W. P. Raney, "Attenuation in Shallow-Water Propagation due to an Absorbing Bottom," J. Acoust. Soc. Am. 27, 689-692 (1955).

27. M. C. Ferla, G. Dreini, F. B. Jensen, and W. A. Kuperman, "Broadband, Model/Data Comparisons for Acoustic Propagation in Coastal Waters," in Bottom-Interacting Ocean Acoustics, edited by W. A. Kuperman and F. B. Jensen (Plenum Press, New York, 1980), pp. 577-592.

28. S. G. Payne, C. Penland, and R. Gonzalez, "Acoustic Normal Mode Model NEMESIS," Applied Research Laboratories Technical Report No. 81-30 (ARL-TR-81-30), Applied Research Laboratories, The University of Texas at Austin, in preparation.

29. R. Gonzalez and S. G. Payne, "User's Manual for NEMESIS and PLMODE," Applied Research Laboratories Technical Memorandum No.80-6 (ARL-TM-80-6), Applied Research Laboratories, The University of Texas at Austin, May 1980.

30. C. L. Pekeris, "Theory of Propagation of Explosive Sound in Shallow Water," The Geological Society of America, Memoir 27 (1948).

31. A. O. Williams, "Hidden Depths: Acceptable Ignorance about Ocean Bottoms," J. Acoust. Soc. Am. 59, 1175-1179 (1976).

RELATED PUBLICATIONS

Publications

A. L. Anderson and K. C. Focke, "Model Sensitivity Studies: Ambient Noise Depth Dependence Related to Propagation Loss" (U), U.S. Navy Journal of Underwater Acoustics 28, 219-228 (1978) (ARL-TP-77-21, May 1977). (CONFIDENTIAL)

K. C. Focke and D. E. Weston, "Problems of the Caustics in Range-Averaged Ocean Sound Channels," submitted to J. Acoust. Soc. Am. for publication, 1980.

S. K. Mitchell and K. C. Focke, "The Role of the Seabottom Attenuation Profile in Shallow Water Acoustic Propagation," submitted to J. Acoust. Soc. Am. for publication, July 1982.

S. K. Mitchell and K. C. Focke, "New Measurements of Compressional Wave Attenuation in Deep Ocean Sediments," J. Acoust. Soc. Am. 67, No. 5 (1980) (ARL-TP-79-33, August 1979).

Reports

A. L. Anderson, R. L. Deavenport, and K. C. Focke, "Propagation Loss Calculations with a Normal Mode Propagation Model Using an Epstein Curve Fitted to Existing Cayman Trough Sound Speed versus Depth Profiles," Applied Research Laboratories Technical Memorandum No. 72-36 (ARL-TM-72-36), Applied Research Laboratories, The University of Texas at Austin, November 1972.

K. C. Focke and S. K. Mitchell, "Estimates of Passive Acoustic Detection in the Southwest Approaches to the English Channel" (U), Applied Research Laboratories Technical Report No. 81-39 (ARL-TR-81-39), Applied Research Laboratories, The University of Texas at Austin, August 1981. (CONFIDENTIAL)

K. C. Focke, J. A. Shooter, N. R. Bedford, and S. K. Mitchell, "CHURCH STOKE II-Cruise 5 PAR/ACODAC Environmental Acoustic Measurements and Analysis" (U), Applied Research Laboratories Technical Report No. 79-52 (ARL-TR-79-52), Applied Research Laboratories, The University of Texas at Austin, October 1979. (CONFIDENTIAL)

T. L. Foreman, K. C. Focke, and K. E. Hawker, "A Status Report on Propagation Loss and Bottom Loss Models in Use at ARL:UT," Applied Research Laboratories Technical Memorandum No. 77-1 (ARL-TM-77-1), Applied Research Laboratories, The University of Texas at Austin, February 1977.

A. L. Anderson and K. C. Focke, "Propagation Model Predictions Technical Note," Applied Research Laboratories Technical Memorandum No. 73-8 (ARL-TM-73-8), Applied Research Laboratories, The University of Texas at Austin, April 1973.

A. L. Anderson, L. D. Hampton, and K. C. Focke, "Low Frequency Sound Propagation in the Cayman Trough," Applied Research Laboratories Technical Report No. 73-59 (ARL-TR-73-59), Applied Research Laboratories, The University of Texas at Austin, November 1973.

K. E. Hawker, A. L. Anderson, K. C. Focke, and T. L. Foreman, "Initial Phase of a Study of Bottom Interaction of Low Frequency Underwater Sound," Applied Research Laboratories Technical Report No. 76-14 (ARL-TR-76-14), Applied Research Laboratories, The University of Texas at Austin, April 1976.

K. E. Hawker, K. C. Focke, and A. L. Anderson, "A Preliminary Sensitivity Study of Underwater Sound Propagation Loss and Bottom Loss," Applied Research Laboratories Technical Report No. 77-17 (ARL-TR-77-17), Applied Research Laboratories, The University of Texas at Austin, February 1977.

K. C. Focke and M. W. Ohlendorf, "The Minifact Module," Applied Research Laboratories Technical Memorandum No. 77-20 (ARL-TM-77-20), Applied Research Laboratories, The University of Texas at Austin, August 1977.

"Results of a Study on the Bottom Interaction of Underwater Sound," (with K. E. Hawker, S. R. Rutherford, W. E. Williams, T. L. Foreman, and R. Gonzalez), Applied Research Laboratories Technical Report No. 77-27 (ARL-TR-77-27), Applied Research Laboratories, The University of Texas at Austin, October 1977.

K. C. Focke and L. A. Shurr, "BEARING STAKE Exercise Reconstruction Charts" (U), Applied Research Laboratories Technical Memorandum No. 78-3 (ARL-TM-78-3), Applied Research Laboratories, The University of Texas at Austin, June 1978. (CONFIDENTIAL)

S. K. Mitchell, K. C. Focke, J. J. Lemmon, and M. M. McSwain, "Analysis of Acoustic Bottom Interaction in BEARING STAKE" (U), Applied Research Laboratories Technical Report No. 79-24 (ARL-TR-79-24), Applied Research Laboratories, The University of Texas at Austin, February 1979. (CONFIDENTIAL)

S. K. Mitchell, K. C. Focke, J. A. Shooter, and N. R. Bedford, "BEARING STAKE - Vertical ACODAC Acoustic Measurements Data Report" (U), Applied Research Laboratories Technical Report No. 78-8 (ARL-TR-78-8), Applied Research Laboratories, The University of Texas at Austin, February 1978. (CONFIDENTIAL)

A. L. Anderson, K. C. Focke, and D. J. Shirley, "Model Studies of Fluctuations of Interfering Direct and Surface Reflected Pulses," Applied Research Laboratories Technical Report No. 73-38 (ARL-TR-73-38), Applied Research Laboratories, The University of Texas at Austin, 31 July 1973.

Presentations

"Model Sensitivity Studies: Ambient Noise Depth Dependence Related to Propagation Loss " (U), presented at the 31st U.S. Navy Symposium on Underwater Acoustics, San Diego, California, November 1976. (CONFIDENTIAL)

"Estimates of Passive Acoustic Detection in the Southwest Approaches to the English Channel" (U), to be presented at the Sonar Technology Panel, GPT-9 of Subgroup G Meeting in Salisbury, Australia, October 1982. (CONFIDENTIAL)

"Estimation of Attenuation Profiles in Shallow Water Regions" (U), to be presented at the Sonar Technology Panel, GPT-9 of Subgroup G Meeting in Salisbury, Australia, October 1982. (CONFIDENTIAL)

Estimates of Passive Acoustic Detection in the Southwest Approaches to the English Channel" (U), presented at 1982 Undersea Surveillance Symposium in Monterey, California, July 1982.

29 February 1984

DISTRIBUTION LIST FOR
ARL-TR-84-6
UNDER CONTRACT N00014-82-K-0015

Copy No.

Commanding Officer
Naval Ocean Research and Development Activity
NSTL Station, MS 39529
1 Attn: E. D. Chaika (Code 530)
2 R. Gardner (Code 501)
3 D. B. King (Code 321)
4 W. A. Kuperman (Code 320)
5 CDR M. McCallister (Code 522)
6 R. Martin (Code 110A)
7 J. Matthews (Code 362)
8 W. W. Worsley (Code 110A)

Chief of Naval Research
Department of the Navy
Arlington, VA 22217
9 Attn: M. McKisic (Code 425-OA)
10 R. Obrochta (Code 425 AR)

Office of Naval Research Detachment
Naval Ocean Research and Development Activity
NSTL Station, MS 39529
11 Attn: G. Morris (Code 425GG)

Commanding Officer
Naval Electronic Systems Command
Department of the Navy
Washington, D.C. 20360
12 Attn: LCDR S. Hollis (Code 612)
13 R. Mitnick (Code 612)
14 CDR C. Spikes (PDE 124-60)
15 L. Parish (PDE 124-50)

Director
Naval Research Laboratory
Department of the Navy
Washington, D.C. 20375
16 Attn: B. B. Adams (Code 8160)

Distribution list for ARL-TR-84-6 under Contract N00014-82-K-0015 (cont'd)

Copy No.

Commanding Officer
Naval Ocean Systems Center
Department of the Navy
San Diego, CA 92152
17 Attn: E. L. Hamilton
18 M. A. Pederson
19 H. P. Bucker

Commander
Naval Sea System Command
Department of the Navy
Washington, D.C. 20362
20 Attn: C. D. Smith (Code 63R)
21 D. E. Porter (Code 63R1)

Chief of Naval Operations
Department of the Navy
Washington, D.C. 20350
22 Attn: CAPT E. Young (OP 952D)

Chief of Naval Material
Department of the Navy
Washington, D.C. 20360
23 Attn: CAPT J. Harlett (MAT 0724)

24 Commander
Naval Surface Weapons Center
White Oak Laboratory
Department of the Navy
Silver Spring, MD 20910

25 Commander
David W. Taylor Naval Ship Research and
Development Center
Department of the Navy
Bethesda, MD 20034

Naval Oceanographic Office
Department of the Navy
NSTL Station, MS 39522
26 Attn: W. Jobst (Code 7300)
27 J. Allen (Code 7310)
28 R. Hecht (Code 7332)

Distribution list for ARL-TR-84-6 under Contract N00014-82-K-0015 (cont'd)

Copy No.

39 - 50 Commanding Officer and Director
Defense Technical Information Center
Cameron Station, Building 5
5010 Duke Street
Alexandria, VA 22314

Woods Hole Oceanographic Institution
86-95 Water Street
Woods Hole, MA 02543
51 Attn: R. Spindel

Science Applications, Inc.
1710 Goodridge Drive
McLean, VA 22101
52 Attn: C. Spofford
53 J. Hanna

Applied Research Laboratory
The Pennsylvania State University
P. O. Box 30
State College, PA 16801
54 Attn: S. McDaniel

Marine Physical Laboratory of
The Scripps Institution of Oceanography
The University of California, San Diego
San Diego, CA 92132
55 Attn: F. Fisher
56 G. Shor

Scripps Institution of Oceanography
The University of California, San Diego
La Jolla, CA 92037
57 Attn: Library
58 R. Tyce

Bell Telephone Laboratories, Inc.
Whippany Road
Whippany, NJ 07961
59 Attn: A. Carter
60 R. Holford
61 D. Romain

Planning Systems, Inc.
7900 Westpark Drive, Suite 507
McLean, VA 22101
62 Attn: R. Cavanaugh
63 B. Brunson

Distribution list for ARL-TR-84-6 under Contract N00014-82-K-0015 (cont'd)

Copy No.

Commander
Naval Air Development Center
Department of the Navy
Warminster, PA 18974
29 Attn: C. L. Bartberger

Officer in Charge
New London Laboratory
Naval Underwater Systems Center
Department of the Navy
New London, CT 06320
30 Attn: B. Cole
31 F. R. DiNapoli
32 P. Herstein

33 Director Naval Warfare
Deputy Undersecretary Defense R&E
Room 3D1048, Pentagon
Washington, D.C. 20301

OASN (R,E&S)
Room 4D745, Pentagon
Washington, D.C. 20301
34 Attn: G. A. Cann

Superintendent
Naval Postgraduate School
Monterey, CA 93940
35 Attn: Library

Commander
Naval Coastal Systems Center
Department of the Navy
Panama City, FL 32407
36 Attn: G. McLeroy

Defense Advanced Research Projects Agency
1400 Wilson Blvd.
Arlington, VA 22209
37 Attn: CDR K. Evans (TTO)

38 Commander
Naval Intelligence Support Center
4301 Suitland Road
Washington, D.C. 20390

Distribution list for ARL-TR-4-6 under Contract N00014-82-K-0015 (cont'd)

Copy No.

TRW, Inc.
TRW Defense & Space Systems Group
Washington Operations
7600 Colshire Drive
McLean, VA 22101
64 Attn: R. T. Brown
65 I. Gereben

Defence Scientific Establishment
HMNZ Dockyard
Devonport, Auckland
NEW ZEALAND
66 Attn: K. M. Guthrie

School of Mechanical Engineering
Georgia Institute of Technology
Atlanta, GA 30332
67 Attn: A. D. Pierce

Department of Geology and Geophysics
Geophysical and Polar Research Center
Lewis G. Weeks Hall for Geological Sciences
The University of Wisconsin, Madison
1215 W. Dayton Street
Madison, WI 53706
68 Attn: C. S. Clay

Courant Institute
251 Mercer Street
New York, NY 10012
69 Attn: D. C. Stickler

Bolt, Beranek, & Newman, Inc.
50 Moulton Street
Cambridge, MA 02138
70 Attn: H. Cox

Hawaii Institute of Geophysics
The University of Hawaii
2525 Correa Road
Honolulu, HI 96822
71 Attn: L. N. Frazer

Director
North Atlantic Treaty Organization
SACLANT ASW Research Centre
APO New York 09019
72 Attn: T. Akal

Distribution list for ARL-TR-84-6 under Contract N00014-82-K-0015 (cont'd)

Copy No.

Defence Research Establishment Pacific
FMO Victoria, BC
VOS 1BO CANADA
73 Attn: R. Chapman

Defence Research Establishment Atlantic
9 Grove Street
P. O. Box 1012
Dartmouth, NS
CANADA
74 Attn: D. Chapman

Rosenteil School of Marine and
Atmospheric Science
The University of Miami
10 Rickenbacker Causeway
Miami, FL 33149
75 Attn: H. DeFarrari

Applied Physics Laboratory
The Johns Hopkins University
Johns Hopkins Road
Laurel, MD 20810
76 Attn: J. Lombardo
77 R. Henrick

Department of Ocean Engineering
Massachusetts Institute of Technology
Cambridge, MA 02139
78 Attn: I. Dyer
79 G. Duckworth
80 A. Baggerar

The University of Miami
10 Rickenbacker Causeway
Miami, FL 33149
81 Attn: F. Tappert

Physics Department
The University of Rhode Island
Kingston, RI 02881
82 Attn: C. Kaufman

Department of Electrical Engineering
Polytechnic Institute of New York
Farmingdale, NY 11735
83 Attn: L. B. Felsen

Distribution list for ARL-TR-84-6 under Contract N00014-82-K-0015 (cont'd)

Copy No.

84 I. Tolstoy
Knockvennie, Castle Douglas
S. W. SCOTLAND
GREAT BRITAIN

Department of Geology
The University of Texas at Austin
Austin, TX 78712
85 Attn: C. Wilson

Physics Department
The University of Auckland
Private Bag, Auckland
NEW ZEALAND
86 Attn: A. C. Kibblewhite
87 C. T. Tindle

Chinhae Research Laboratory
P. O. Box 18
Chinhae, Kyeong Nam
KOREA
88 Attn: Jungyul Na

The Lamont-Doherty Geological Observatory
Columbia University
Palisades, NY 10964
89 Attn: R. D. Stoll

Ocean Data Systems, Inc.
Defense Systems
6110 Executive Blvd., Suite 320
Rockville, MD 20852
90 Attn: G. Jacobs
91 P. C. Etter

92 Nancy R. Bedford, ARL:UT

93 Glen E. Ellis, ARL:UT

94 Karl C. Focke, ARL:UT

95 Terry L. Foreman, ARL:UT

96 Robert F. Gragg, ARL:UT

97 Loyd Hampton, ARL:UT

98 Kenneth E. Hawker, ARL:UT

Distribution list for ARL-TR-84-6 under Contract N00014-82-K-0015 (cont'd)

Copy No.	
99	Stephen G. Houser, ARL:UT
100	Jo B. Lindberg, ARL:UT
101	Robert A. Koch, ARL:UT
102	David Knobles, ARL:UT
103	Stephen K. Mitchell, ARL:UT
104	David W. Oakley, ARL:UT
105	Clark S. Penrod, ARL:UT
106	Richard Pitre, ARL:UT
107	Carol V. Sheppard, ARL:UT
108	Paul J. Vidmar, ARL:UT
109	Library, ARL:UT
110-120	Reserve, ARL:UT

END

FILMED

6-84

DTIC